ACS NANO

www.acsnano.org



ARTICLE

# Vibronically Coherent Exciton Trapping in Monolayer $WS_2$

Yorrick Boeije, Anh Tuan Hoang, Juhwan Lim, Samuel D. Stranks, Manish Chhowalla, Eric Pop, Andrew J. Mannix, and Akshay Rao*

Cite This: *ACS Nano* 2025, 19, 26942−26952

Read Online

ACCESS | Metrics & More | Article Recommendations | Supporting Information

**ABSTRACT:** **Defect engineering in transition metal dichalcogenide (TMD) monolayers enables applications in single-photon emission, sensing, and photocatalysis. These functionalities critically depend on defect type, density, spatial distribution, relative energy, and the dynamics of exciton trapping at the defect sites. The latter are mediated by coupling to optical phonons through mechanisms not yet fully understood. Traditionally, exciton or carrier trapping at defects in inorganic crystals has been described by incoherent multiphonon emission within the Born−Oppenheimer approximation—an approach that underpins the widely used Shockley−Read−Hall framework for nonradiative recombination. Here, we use impulsive vibrational spectroscopy to investigate exciton trapping in defect-modified monolayers of $WS_2$ grown through metal−organic chemical vapor deposition. We find that the phonon coherences of the Raman-active A' and E' modes persist throughout the ultrafast (∼100 fs) exciton trapping process, indicating a continuous evolution of the excitonic wave function. This observation is consistent with a conical intersection-mediated trapping process, in which a potential energy surface crossing between the free and trapped excitonic states acts as a funnel to drive this nonadiabatic transition. Such a molecular-like, vibronically coherent mechanism lies beyond the Born−Oppenheimer approximation, in stark contrast to classical, incoherent trapping models in solids. Moreover, the faster dephasing of the E' mode in the trapped exciton state compared to the free exciton suggests it acts as a vibrational coordinate that promotes the trapping process. These findings provide mechanistic insights into exciton−phonon interactions at defects in TMD monolayers and inform strategies for engineering quantum and energy functionalities.**

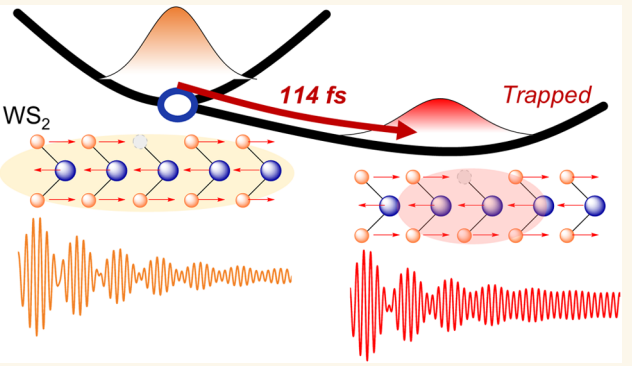


**KEYWORDS:** *transition metal dichalcogenide defects, exciton trapping, conical intersections, vibronic coherence, exciton−phonon coupling, defect engineering, defect photophysics*



Defects are imperfections in crystal lattices that have historically been regarded as unwanted, hampering optoelectronic device performances in photovoltaics and light-emitting diodes by facilitating nonradiative recombination and reducing charge carrier mobilities. However, their inherently localized nature could be used to drive energy transfer[1] and photochemistry[2] for catalysis-based energy technologies or for single photon emission[3] in quantum technologies. Two-dimensional (2D) transition metal dichalcogenides (TMDs) have emerged as a class of materials that could take advantage of such defect functionalities.[4] The performance of defect-engineered TMD monolayers hinges on a deeper understanding of defect-specific exciton−phonon coupling, which is the main decoherence channel in single photon emitters,[5−7] as well as the exciton trapping and recombination dynamics at those defects. Just as multiphonon emission models are used to describe free carrier trapping and nonradiative recombination (i.e., Shockley-Read-Hall processes)[13−16] at deep defects in bulk semiconductors, similar theoretical frameworks have been developed to describe exciton trapping in TMDs.[17,18]

Experimental reports typically focus on exciton trapping and trap-related scattering mechanisms in TMDs but do not provide phonon mode-specific detail.[19−23] Mode-specific detail is essential to trace exciton trapping pathways, yet such detail has remained experimentally inaccessible. While Raman studies

Received: May 22, 2025
Revised: June 17, 2025
Accepted: July 9, 2025
Published: July 21, 2025





https://doi.org/10.1021/acsnano.5c08533
*ACS Nano* 2025, 19, 26942−26952

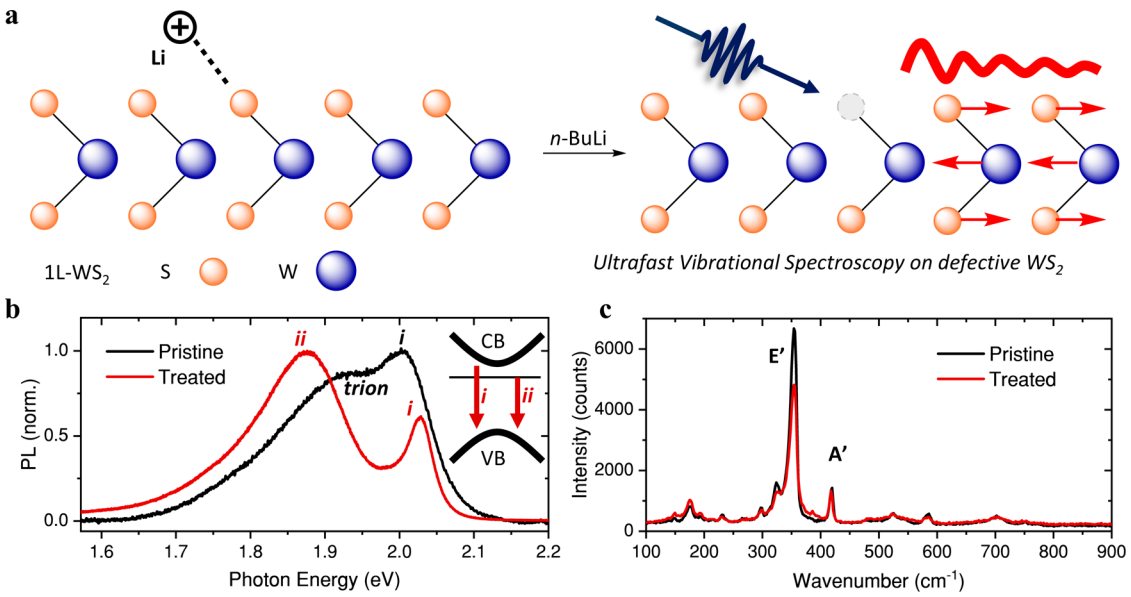


**Figure 1. *n*-BuLi treatment of monolayer $WS_2$induces a bright lower-energy emission. (a) Schematic of *n*-BuLi treatment. The proposed mechanism involves a positively charged lithium ion extracting a sulfur atom, leaving a sulfur vacancy. The interaction of vibrations with the defects are studied with ultrafast impulsive vibrational spectroscopy (IVS) in this work. (b) Photoluminescence spectra of pristine and treated $WS_2$. The assigned emission peaks of the treated film are indicated in the inset. CB: conduction band. VB: valence band. (c) Steady-state Raman spectra of pristine and treated $WS_2$. Optical measurements are taken at room temperature.**

offer phonon mode detail and, in some cases, can reveal local defect-induced modes,[24] they are limited to ground-state structural characterization. Time-resolved pump−probe approaches offer the capability to study interaction of defects with phonons in the time domain, demonstrating a clear link between defect density and phonon dephasing[25,26] and mode-selective interactions with defects.[27,28] However, these experiments typically do not probe the full excited state absorption spectrum.

In this study, we employ broadband impulsive vibrational spectroscopy (IVS) to elucidate the mechanism of exciton trapping in TMD monolayers. IVS uniquely enables broadband probing of excited state vibrational modes[29,30] and has proven powerful to identify key modes in ultrafast photochemical reactions,[31] nonradiative decay in organic light emitting diodes[32] and polaron formation in hybrid perovskites,[33] yet it has not been applied to shine light on exciton/carrier trapping mechanisms.

Through a controlled, short-duration *n*-butyl-lithium (*n*-BuLi) treatment on $WS_2$ monolayers grown by metal−organic chemical vapor deposition (MOCVD), we engineer a defect-rich model system tailored for a comprehensive study of exciton trapping at defect sites. The phonon coherences of the Raman-active A' and E' modes survive the ultrafast (∼100 fs) trapping process, indicating a continuous evolution of the exciton wave function. We demonstrate that vibronically coherent trapping is consistent with a conical intersection-mediated mechanism, where a crossing between potential energy surfaces associated with the free and trapped excitonic states acts as a funnel to drive the nonadiabatic transition. This interpretation is supported by the energetically distinct and bright defect emission, as well as the faster dephasing of E' in trapped vs free excitonic population. These findings not only enhance our fundamental understanding of exciton−phonon interactions at defects but also provide critical insights for defect engineering strategies.

## RESULTS

The preparation of untreated and *n*-BuLi treated MOCVD[34] $WS_2$ monolayer is described in the Methods section and schematically illustrated in Figure 1a. In addition to the well-known exciton A emission at 2.03 eV (*i* in Figure 1b), the *n*-BuLi treatment introduces a lower-energy emission (*ii* 1.88 eV) in the steady-state photoluminescence spectrum under ambient conditions (Figure 1b). In previous reports, the appearance of such a lower-energy bright emission after both annealing and chemical treatments have been assigned to defect excitons localized at sulfur vacancies,[35−37] which introduce deep acceptor levels.[36,38,39] Even though due to thermodynamic considerations it is expected that most sulfur vacancies will be filled with oxygen upon air exposure,[40] it has been shown for $MoS_2$ films with postgrowth treatment that sulfur vacancies can still persist at sufficiently high densities ($>1 \times 10^{14}$ $cm^{-2}$).[35,41] Importantly, oxygen substituted defects typically result in a blueshift of the exciton emission,[42] as their levels align with the $WS_2$ valence band, rather than the ∼0.2 eV red-shifted emission peak in this work and $MoS_2$.[35] Given the smaller energy separation relative to the *i* and *ii* emission peaks observed in the treated film, we assign the shoulder peak (1.95 eV) in the pristine film spectrum to trion emission, rather than defect-related emission, as previously reported for pristine films.[43] Consistent with a reduction in trion population due to a suppressed n-type doping,[36,42] the exciton A emission sharpens and exhibits a ∼30 meV blueshift following *n*-BuLi treatment. Based on the unchanged positions of the A' and E' Raman modes at 419 $cm^{-1}$ and 355 $cm^{-1}$ (Figure 1c), respectively, which match literature-reported $WS_2$-monolayer spectra of the 2H phase,[44,45] we can exclude any treatment induced phase change. The similar PL and Raman spectra of a *n*-BuLi treated mechanically exfoliated $WS_2$ film illustrates the general applicability of this defect engineering method (Figure S1).



https://doi.org/10.1021/acsnano.5c08533
ACS Nano 2025, 19, 26942−26952

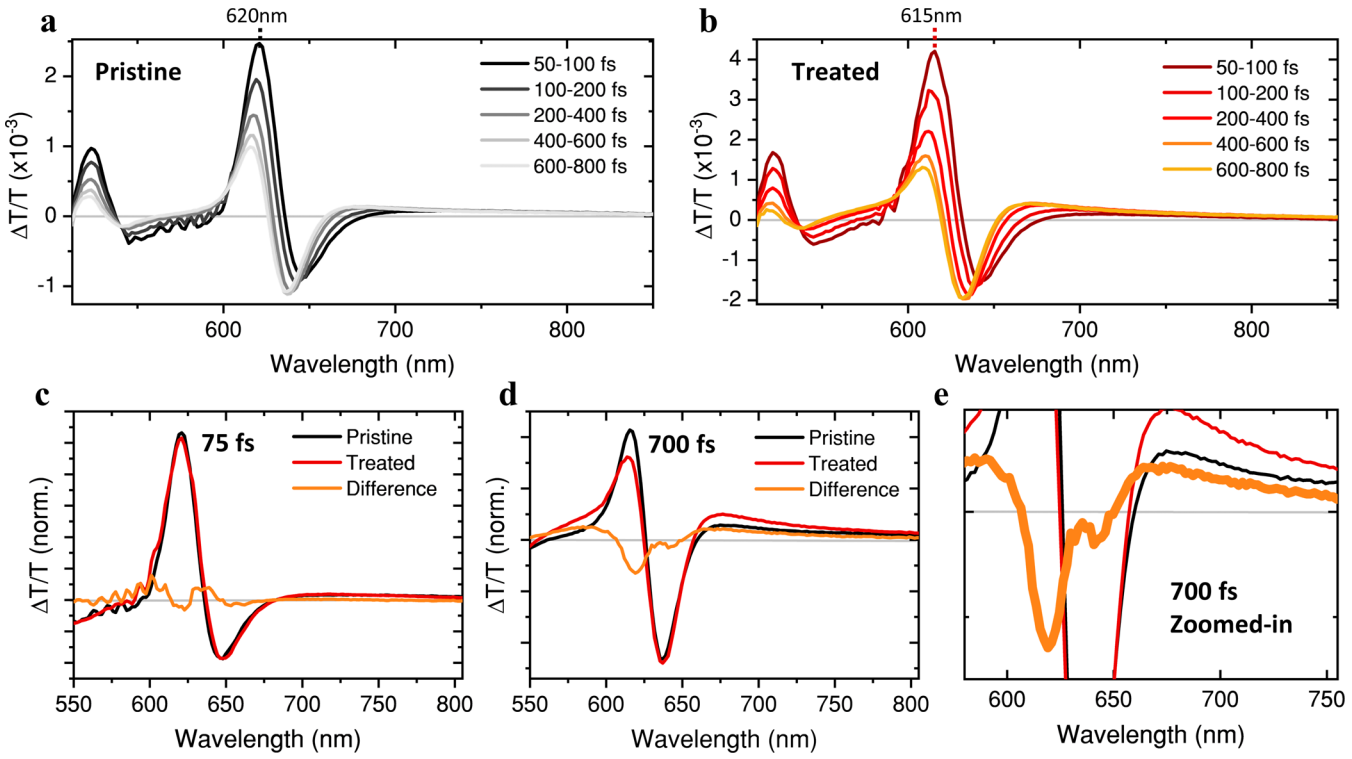


**Figure 2. Ultrafast exciton trapping. (a) Femtosecond temporal evolution of the transient absorption spectra for a pristine $WS_2$ film. (b) Transient absorption spectra for a *n*-BuLi treated $WS_2$ film. (c) Difference spectra (after normalization of the full TA map) for both films at 75 fs. (d) Difference spectra at 700 fs. (e) Zoomed-in view of (d). The spectra in (c) and (d) are aligned to the exciton A bleach of the pristine film to account for the treatment-induced 5 nm blueshift. From the difference spectra the treatment induces a faster exciton A decay (600−625 nm), as well as a stronger lower-energy bleach (670−720 nm).**

The transient absorption (TA) spectra of a pristine and a treated $WS_2$ film are shown in Figure 2a,2b. The 600−625 nm spectral region is dominated by the exciton A bleach, and the 510−530 nm by the exciton B bleach, consistent with previously reported TA studies on monolayer $WS_2$.[46−48] To emphasize spectral differences between treated and pristine $WS_2$ their differences (treated − pristine) are plotted in Figure 2c,2d, at 75 and 700 fs, respectively. The treatment induces a blueshift in the exciton A bleach, in agreement with the blueshift observed in the A exciton emission in Figure 1b, while the exciton B bleach remains unaffected. We took this blueshift into account by aligning the exciton A bleach of treated to pristine prior to subtraction, enabling a clearer comparison of relative bleach intensities. Importantly, right after photoexcitation (75 fs) the treated and pristine spectra are nearly identical, while the 700 fs difference spectrum shows a reduced exciton A bleach and an enhanced lower-energy bleach (670−720 nm) associated with the *n*-BuLi-treatment, consistent with ultrafast exciton trapping. A similar sub-ps growth of a subgap bleach has been observed by Bretscher et al.[36] in sulfur vacancy containing $MoS_2$. The broad 670−720 nm bleach agrees with the appearance of lower-energy emission feature (Figure 1b) corresponding to defect transitions.

We focused our analysis on the spectral region corresponding to the A exciton bleach—hereafter referred to as the free exciton (Figure 3a)—rather than the exciton B bleach, due to lower signal-to-noise ratio of the latter. Although the trapped exciton bleach likely extends to wavelengths shorter than 670 nm, similar to what is observed in the defect emission, we limit our analysis to the 670−720 nm spectral region, where the TA signal is dominated by the trapped exciton.

Figure 3b shows the normalized kinetic traces of both free (orange) and trapped (red) excitons. As the free exciton bleach decreases in intensity, the trapped exciton signal increases. The latter is fitted to a biexponential function with time constants of $\tau_1$ = 114 fs and $\tau_2$ = 1.3 ps, that represent the trapping and recombination time scales, respectively. The trapping lifetime is slightly shorter than previously reported for untreated $WS_2$ (~300−400 fs),[47,49] but notably shorter than that observed in $MoS_2$ (1−2 ps).[23,36] The concomitant reduction in the free exciton A signal and increase in trapped exciton signal supports the assignment of the emerging spectral features to excitons trapped at defect sites.

The kinetics in Figure 3b reveal oscillations superimposed on the electronic dynamics. The electronic dynamics are removed by the biexponential fit to acquire the pure oscillatory traces for the free and trapped excitons in Figure 3c,3d, respectively. These ~80 fs period oscillations represent phonon coherences generated by the ultrafast pump (10 fs), which modulate the transient absorption spectrum in time. Strikingly, the conservation of phonon coherence during the exciton trapping process is inconsistent with an incoherent, hopping-like mechanism, which would be expected to destroy any phonon coherence.[50−53] A closer inspection of the first 300 fs reveals a ~25 fs delay in the buildup of coherence associated with trapping (Figure 3e), suggesting a trapping-mediated transfer of coherence. The fast Fourier transform (FFT) of these oscillations reveal both the Raman-active E' (356 $cm^{-1}$) and A' (420 $cm^{-1}$) modes (Figure 3f), and are close to the ground-state Raman mode frequencies (Figure


https://doi.org/10.1021/acsnano.5c08533
ACS Nano 2025, 19, 26942−26952

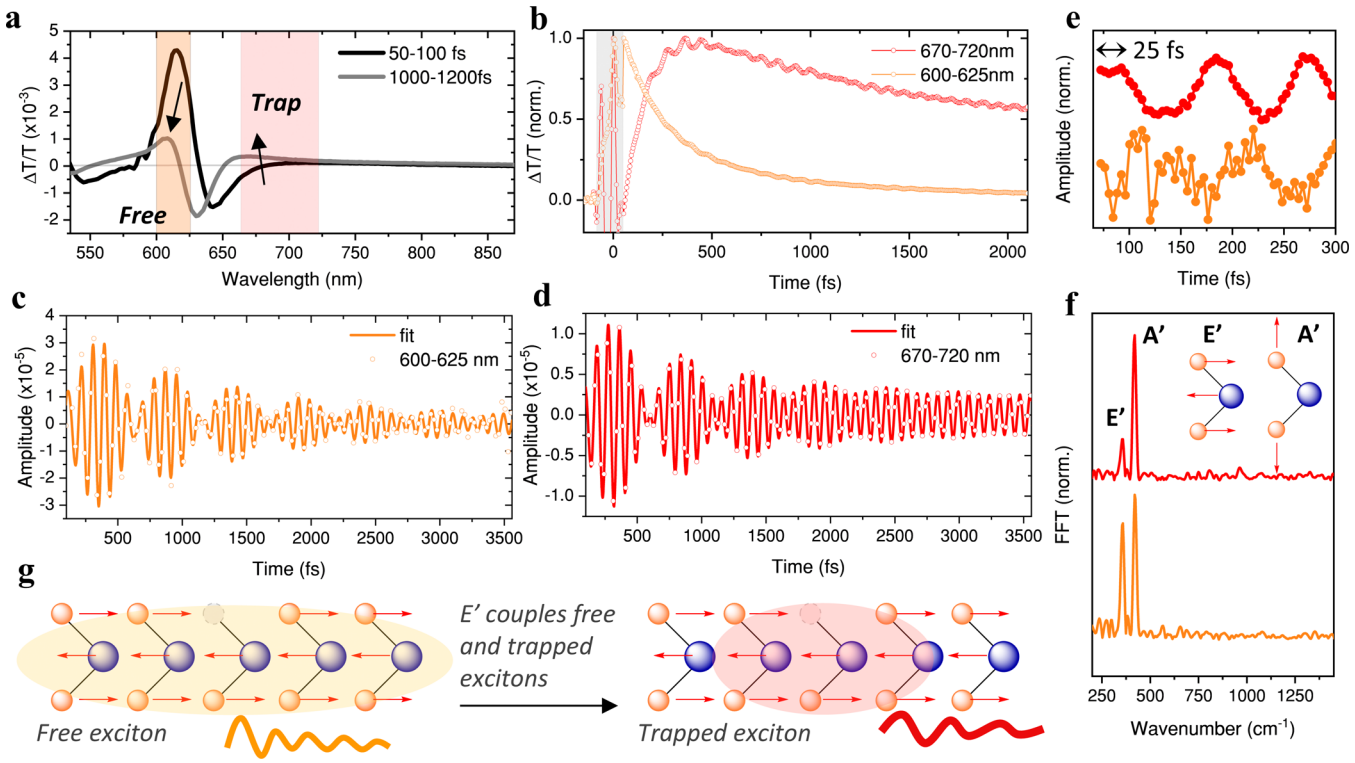


**Figure 3. Exciton trapping modulates phonon coherences. (a) Transient absorption spectra of *n*-BuLi treated $WS_2$ monolayer. (b) Kinetics integrated between 600−625 nm (free exciton in orange) and 670−720 nm (trapped exciton in red). Gray transparent box indicates coherent artifact. (c) Electronic-decay free oscillation and its corresponding damped sinusoid function fit for the free exciton. (d) Electronic-decay free oscillation and its corresponding damped sinusoid function fit for the trapped exciton. (e) Early time scale electronic-decay free oscillations. (f) Fast Fourier transform (FFT) over the complete time range. (g) Schematic 1D illustration of the coupling/promoting role of the E' mode to drive exciton trapping.**

1c). The assignment of the A' mode is further discussed in Supporting Note 1 (Figures S2−S4).

We now analyze the phonon coherences in more detail to elucidate the physical interpretation of the conserved coherence. We fitted the electronic-decay free oscillatory traces to a sum of two exponentially damped sinusoid functions (eq 1)

$$f(t) = A_1 e^{-t/\tau_1}\sin(2\pi \times \omega_1 t - \phi_1) + A_2 e^{-t/\tau_2}\sin(2\pi \times \omega_2 t - \phi_2) \quad (1)$$

Where $A_1$ and $A_2$ represent the amplitudes, $\omega_1$ and $\omega_2$ the frequencies, $\tau_1$ and $\tau_2$ the dephasing times (often loosely referred to as "lifetimes"), and $\phi_1$ and $\phi_2$ the phases, of the A' and E' oscillations, respectively. The fitted parameters are provided in Table 1 and the residuals in Figure S5.

**Table 1. Damped Sinusoid Fitting Results[a]1**

| mode i (spectrum) | $\nu_i$ ($cm^{-1}$) | $A_i$ ($\times 10^{-5}$) | $\tau_i$ (fs) | $\phi_i$ (rad) |
|---|---|---|---|---|
| A' (free) | 420 ± 0.3 | 1.3 ± 0.08 | [b]2386 ± 392 | 4.4 ± 0.06 |
| A' (trap) | 419 ± 0.1 | 0.5 ± 0.01 | [b]4770 ± 454 | 1.6 ± 0.03 |
| E' (free) | 356 ± 0.3 | 2.8 ± 0.12 | 980 ± 57 | 6.1 ± 0.04 |
| E' (trap) | 356 ± 0.3 | 1.0 ± 0.03 | 741 ± 30 | 4.0 ± 0.03 |

[a]The electronic-decay free oscillatory traces in Figure 3c,d are fitted to equation 1. [b]Due to the limited temporal measurement range, this value should be interpreted with caution.

Traditionally, phonon dephasing has contributions from defect-phonon scattering induced by the local potential ($\tau_{defect}$), phonon−phonon scattering through anharmonicity ($\tau_{anharmonic}$) and phonon-carrier scattering ($\tau_{carrier}$),[25] resulting in a total dephasing time $(\tau_{total})^{-1} = (\tau_{defect})^{-1} + (\tau_{anharmonic})^{-1} + (\tau_{carrier})^{-1}$. The fitting provides two key observations: (1) the E' mode dephases faster (980 fs for free exciton) compared to the A' mode (2.4 ps) (2) Trapping induces a faster dephasing of E' (741 fs). Our sliding window FFT analysis (Figure S6) supports both observations. The fittings were repeated for more spectral ranges with their parameters provided in Figure S7.

The faster dephasing of the E' mode compared to the A' may arise from their distinct symmetries. As an in-plane vibrational mode, E' may be expected to couple more strongly to local defects than the out-of-plane A' mode, leading to more rapid dephasing.[54] This is analogous to the faster dephasing of C−H stretching compared to C−H bending in a diamond nitrogen-vacancy center.[28] However, optical phonon lifetimes in TMD monolayers are typically on the order of a few picoseconds[55−57] and are primarily governed by optical-acoustic phonon scattering.[58,59] In this context, the E' mode may exhibit shorter lifetimes due to its more efficient phonon−phonon Umklapp scattering enabled by its greater sensitivity to in-plane strain compared to the A' mode.[60] Depending on excitation conditions, phonon-carrier[61−63] scattering may also contribute to the phonon dephasing. For example, phonon-carrier induced fast dephasing could explain the absence of the E' mode in the on-resonant FFT spectra of $MoS_2$[55] and $WSe_2$.[56] For $MoS_2$, the E' mode lifetime increases to 7 ps


https://doi.org/10.1021/acsnano.5c08533
ACS Nano 2025, 19, 26942−26952

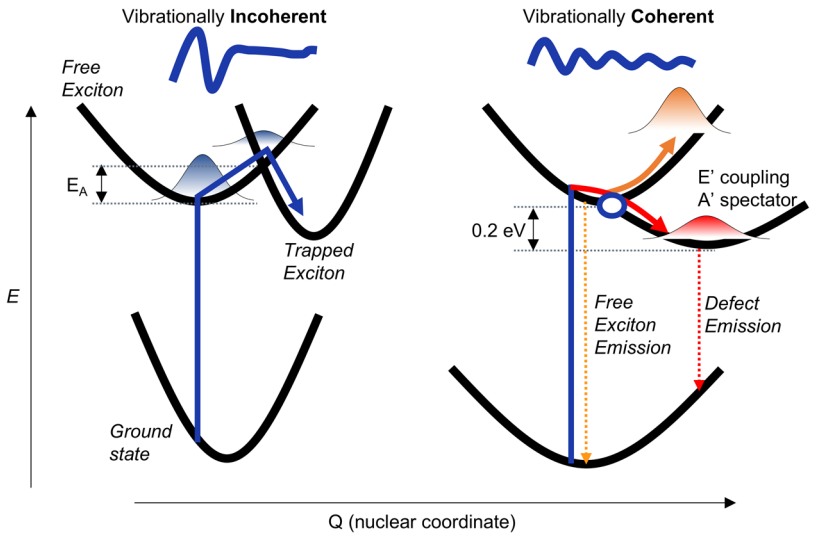


**Figure 4. Configuration coordinate diagram for ultrafast coherent exciton trapping. In the case of traditional thermally activated trapping, an activation barrier ($E_A$) precedes the surface crossing leading to an incoherent process. For a barrierless trapping the coherence generated in the free excitonic state may be transferred to the trapped excitonic state. Coupling modes experience stronger dephasing than tuning or spectator modes as they nonadiabatically couple the free and trapped excitonic states via a conical intersection (indicated with a blue circle). Conventionally, modes that couple trapped to free states are classified as promoter modes, whereas modes absorbing the excess energy as a result of trapping are called accepting modes.**

under off-resonant conditions.[64] Anisotropic electronic distributions and their corresponding momentum relaxation processes correlate with short lifetimes for nonsymmetric modes.[61]

Whereas phonon−phonon (anharmonic) and phonon-defect contributions may in principle be decoupled with temperature and defect density dependence,[25] respectively, broadband IVS enables spectral selectivity of phonon-carrier scattering. As such, we can conclude that the exciton trapping induces a faster E' dephasing (Table 1), either (i) due to an increased exciton−phonon coupling due to the smaller size of the trapped exciton or (ii) because the nonadiabatic transfer associated with trapping causes additional dephasing (Figure 3g). In fact, coupling/promoter modes that drive nonadiabatic transfer experience more rapid dephasing at surface crossings.[52,65−69] Although the A' mode appears to be longer-lived as a result of trapping, the exact lifetime values of the A' mode are not accurate due to the limited temporal range of the measurement. The spectral insensitivity of the A' and E' Raman frequencies indicates that the vibrational manifold is only weakly perturbed by the trapping, implying a similar size of the trapped exciton compared to its free size (∼1−2 nm),[70] consistent with explanation (ii). Indeed, the trapping potential has to be sufficiently broad to capture excitons efficiently.[18] Consistently, we do not observe any local defect-related modes, in contrast to the IVS results on $MoSe_2$ from Bae et al.[71]

Electron and hole trapping at defect sites has been traditionally described by a multiphonon emission process involving "promoting" (or coupling) and "accepting" modes that couple the delocalized charge carrier to the defect state and accept the excess energy released by this process, respectively (Figure 4).[14,16,72] This mechanism allows non-radiative transitions between states with energy differences much larger than a single available phonon energy to occur. In the present case, the 0.15 eV gap between trapped and free exciton states exceeds any optical phonon mode in $WS_2$. Note that a single mode can act as both a promoting and accepting mode. The first step typically involves an activation barrier and is therefore temperature dependent, making the overall process incoherent. Such a classical picture is not consistent with our observations of ultrafast exciton trapping accompanied by the conservation of phonon coherence.

Instead, we draw inspiration from a mechanistic feature common in molecular photochemistry, a conical intersection, to explain our observations. These are crossings between adiabatic electronic states in nuclear configuration space that enable coherent transfer of vibronic wavepackets.[73−80] Such nonadiabatic transitions inherently involve a breakdown of the Born−Oppenheimer approximation, in stark contrast to the incoherent, thermally activated multi-phonon emission mechanism. While vibronically coherent processes are well-known in molecular systems—such as singlet fission[81] and rhodopsin photoisomerization[82]—they remain largely unexplored in the context of defect trapping in solids. The persistence of vibronic coherence during exciton localization in monolayer $WS_2$ points to a conical intersection-mediated mechanism involving vibronic transfer across the free and trapped excitonic states.

Consistent with vibronic transfer of coherence, there is a build-up time of the trapped exciton phonon coherence, but not in the free exciton phonon coherence (Figure 3e).[83] This delay is associated with a phase shift with respect to the free exciton coherence ($\Delta\phi = 0.9 \pm 0.3\pi$ for A', $\Delta\phi = 0.7 \pm 0.2\pi$ for E' at 100 fs, see Table 1),[83] which also confirms the excited-state nature of the trapped exciton coherence. We further rule out ground-state coherence by the resonance conditions (Supporting Note 1) and the $\sim\pi$ phase flip across the spectrum (Figures S7 and S8).[31,84] Although reaction-driven coherence could be associated with a spectral $\pi$ phase flip as well, we exclude any reaction-driven generation of the coherences[66,67,84,85] in the trapped exciton based on the slower trapping time scale (114 fs) compared to the periods of E' (95 fs) and A' (79 fs) modes. Furthermore, although the trapped and free exciton signals are spectrally convoluted, the node appears to be located in-between these, instead of the maximum of the trapped exciton. Finally, we disregard an


https://doi.org/10.1021/acsnano.5c08533
ACS Nano 2025, 19, 26942−26952

adiabatic vibrationally coherent relaxation mechanism, such as self-trapped exciton formation, to explain our observations. Here, slow dephasing is dominated by phonon−phonon and phonon-defect interactions.[85−88] However, sulfur vacancies introduce midgap states, which can be excited directly (Figure S4), and lead to an additional bright emitting state rather than a single broadened and stokes-shifted emission typically associated with self-trapping.[89,90]

Analogously to the promoting and accepting classification of relevant modes in carrier trapping, conical intersections are characterized by coupling and tuning modes, although with different meanings. The coupling and tuning modes are both promoting in character as they mediate nonadiabatic coupling and the energy gap between the two states, respectively. Coupling modes,[52,65−68] and sometimes in more general vibronic modes,[69] have rather rapid dephasing times due to strong anharmonicities present at the conical intersection,[91] whereas tuning modes or spectator modes (modes without any functional role) are longer-lived.[92,93] The E' mode has the correct symmetry to mediate the in-plane real space shrinking of the free to trapped exciton wave function (Figure 3g) (without any change in wavevector $k$ due to the nondispersive nature of the defect bands[39]) and could therefore have coupling character (Supporting Note 2). The A' mode, on the other hand, vibrates out-of-plane and thus can not couple the two excitonic states (although it does modulate the free excitonic transitions via amplitude modulation as discussed below). These assignments are consistent with their different dephasing behavior. Whereas the large lifetime and the lifetime extension associated with trapping for the A' mode (Table 1) indicates a spectator role, the trapping-enhanced dephasing of E' is consistent with its coupling character.

The distinct relative phases between E' and A' in the trapped exciton population compared to the free exciton population ($\Delta\phi = 0.76\pi$ and $0.54\pi$, respectively at 100 fs) suggest that the transfer of coherence associated with exciton trapping happens at different rates for both modes, confirming their different roles (Table 1 and Figure S7). On the contrary, the phase for both E' and A' remains constant across the exciton A absorption spectral region. This is manifested as an absence of a node at the exciton A maximum (Figure S1), implying *amplitude* modulation[94] of the excitonic transitions via non-Condon effects rather than *frequency* modulation,[95] which has also been observed for exciton C in $MoS_2$.[55] By extrapolating the fitted oscillatory traces to $t = 0$ fs, we can conclude that the A' mode is generated in the displacive limit or via resonant impulsive stimulated Raman scattering (rISRS) as it follows a cosine function (Figure S9).[96] The E' mode is neither a pure impulsive mode, nor a pure displacive mode, based on its 'intermediate phase'. Such an intermediate initial phase indicates a failure of the extrapolation, which assumes no significant changes in electronic population in the first 100 fs and is consistent with its strong coupling to the exciton trapping process. A discussion of unifying Raman theories that can explain these 'intermediate phases'[97−99] is beyond the scope of this article.

To further substantiate the proposed mechanism of vibronically coherent exciton trapping via a defect-induced conical intersection, future theoretical work should aim to explicitly identify such structures in the presence of point defects in TMD monolayers. While defect-induced conical intersections have been studied in medium-sized nanoclusters,[100,101] their role in extended crystalline systems remains largely unexplored. In nanoclusters, defect-induced conical intersections may drive fast nonradiative decay of trapped excitons to the ground state.[100,101] In contrast, trapped excitons in $WS_2$ decay radiatively with long lifetimes[35,37] making such a decay channel unlikely in our case. Finally, we note that the presence of free exciton emission despite the ultrafast trapping time scale is likely a result of the spatial inhomogeneity of the defect distribution, requiring slow carrier diffusion which is outcompeted by emission.

## CONCLUSIONS

In this study, we have used IVS to investigate exciton trapping in chemically treated $WS_2$ monolayers grown by MOCVD. We find that the phonon coherences of the A' and E' Raman modes survive the (~100 fs) trapping process, demonstrating that this process is vibrationally coherent, in contrast to the classical picture of incoherent carrier trapping. This vibrationally coherent process suggests a conical intersection may connect the free and trapped excitonic states, mirroring fast and efficient excitonic processes seen in molecular systems, such as the photoisomerization of rhodopsin which underlies vision. The faster dephasing of the E' mode when coupled to the trapped exciton compared to the free exciton suggests a promoting/coupling role of the trapping process through the conical intersection. Future work should explore how such vibronic pathways depend on layer thickness, type of defect, momentum-space valleys and spatial distribution, and whether they represent a general mechanism for carrier trapping across other low-dimensional materials, bulk semiconductors and nanomaterials—particularly in cases where the trapping occurs on ultrafast time scales.[23,36,102−107] This represents a previously unexplored role for optical phonons in TMDs, which through momentum conservation control moiré interlayer exciton formation,[108] exciton dissociation[109] and emission of indirect excitons.[110] Trapping has been known to induce certain nuclear rearrangements,[105] local defect mode activation[71] and a piezoresponse by triggering acoustic modes,[111] but the dynamical mechanisms of exciton trapping have been rather unexplored experimentally. Point defect vibronic coherences are potential carriers of quantum information and could be exploited for single photon emitters and related light-defect coupled applications.

## METHODS

**Materials.** *MOCVD growth of $WS_2$.* A 4-in. diameter horizontal hot-wall MOCVD system with three heating zones was used for the synthesis of $WS_2$ films on sapphire substrates. Tungsten hexacarbonyl (THC, purity 99.99%, Sigma-Aldrich, 472956) and diethyl sulfide (DES, purity 98%, Sigma-Aldrich, 107247) served as the tungsten and sulfur sources, respectively. A mixture was prepared by dissolving 0.7 g of THC in 100 mL of DES and was stored in a stainless-steel bubbler. An additional supply of DES was kept in a separate bubbler. Both bubblers were maintained at a constant pressure of 800 Torr and room temperature. A Si wafer with 100 nm-thick oxide was horizontally placed in a quartz plate and loaded into the first zone of the furnace after the cleaning process using acetone and isopropanol. Before growth, the system was ramped up to 600 °C for 1 h in a mixture of 1600 sccm of Ar and 20 sccm of $H_2$ at a total pressure of 21.3 Torr. During the growth phase, the flow rate of the carrier gas was reduced to 720 sccm of Ar and 5 sccm of $H_2$, maintaining a pressure of 11.3 Torr. A precise amount of 2 sccm of the THC/DES mixture and 3 sccm of DES were injected into the chamber. After 10 h of growth, the injection of the mixed precursor was halted, and the system was slowly cooled down under 1600 sccm of Ar and 0.5 sccm of $H_2$ while the flow of DES was kept at 0.3 sccm


https://doi.org/10.1021/acsnano.5c08533
ACS Nano 2025, 19, 26942−26952

to minimize the generation of sulfur vacancies. When the system reached 300 °C, the DES line was closed, and the $WS_2$ film remained in the $Ar/H_2$ environment until the system cooled down to room temperature.

*n-Butyllithium Treatment.* $WS_2$ flakes and films were immersed in *n*-butyllithium (1.6 M, Sigma-Aldrich) for 3 h, rinsed with anhydrous hexane (Sigma-Aldrich), and dried. This process was conducted in an $N_2$ glovebox. The treated samples were subsequently washed with deionized water (DI), acetone, and isopropyl alcohol (IPA).

*Mechanical Exfoliation.* Mechanical exfoliation was performed using a PDMS-assisted method. $WS_2$ flakes (2D semiconductor) were exfoliated onto PDMS (Gel-Pak) using blue tape (Ultron Systems, Inc.), and monolayer flakes were identified under an optical microscope. The selected monolayer was then transferred onto ultrathin borosilicate glass.

**Spectroscopy.** *Photoluminescence and Raman Microscopy.* The steady-state Raman measurements were conducted using a Renishaw inVia Raman confocal microscope with a 532 nm excitation laser under ambient conditions. Emission was collected using a 20× long-working-distance objective lens in streamline mode and dispersed by an 1800 l/mm grating with 0.5% of the laser power (<2 $\mu$W).

*Impulsive Vibrational Spectroscopy.* The IVS experiments were performed at room temperature using a custom-built pump−probe setup with a temporal resolution of 10 fs. A broadband white light continuum (WLC) spanning 530−950 nm was generated by pumping a YAG crystal with a 1030 nm fundamental wavelength from a Yb:KGW amplifier laser (Light Conversion Pharos, 14.5 W, 38 kHz repetition rate, 200 fs). This WLC served as the probe beam and was used as a seed to make the pump pulses. The pump beam was produced through noncollinear optical parametric amplification (NOPA) of the 1030-WLC using either the second (515 nm) or third harmonic (343 nm), which were generated by an automatic harmonic generator (Light Conversion HIRO). These pulses achieved durations of 10 fs with spectra spanning 500−650 nm when amplified by the third harmonic, and 11 fs with spectra spanning 650−900 nm when amplified by the second harmonic. Compression of the pump pulses was achieved using chirped mirrors and wedge prisms (Layertec). The spatiotemporal profiles of these pulses were characterized via second-harmonic generation frequency-resolved optical gating (SHG-FROG). Differential transmission spectra were obtained by modulating the pump beam at 9 kHz with a chopper wheel. A computer-controlled piezoelectric translation stage (PhysikInstrumente) with a 4 fs step size was used to set the pump−probe delay. To minimize pump scatter, an ultrabroadband wire grid polarizer (Thorlabs) was placed in the detection path. The transmitted probe was measured using a grating spectrometer equipped with a Silicon camera (Entwicklungsbüro Stresing) operating at 38 kHz and a 550 nm blazed grating. The incident pump fluence was ~ 10 $\mu J/cm^2$, corresponding to an estimated initial carrier density of $n_0 \sim 1.4 \times 10^{12}$ $cm^{-2}$, below the Mott density of $n_{Mott} \sim 2-3 \times 10^{12}$ $cm^{-2}$.[112]

Before the time-domain analysis, background removal and chirp correction were applied to the kinetic traces. Then, biexponential fitting was applied to acquire the electronic-decay free oscillatory traces that represent the phonon coherences. To remove any coherent artifact contributions, these fits were carried out from 70 fs. The resulting traces were either fitted to eq 1 to gain further time-domain information or a FFT analysis was carried out to determine the Raman frequencies. For the first, a 0.01 Hz high-pass fast Fourier transform (FFT) filter was first applied to eliminate artificially low frequencies due to background noise. The FFT analysis was carried out following zero-padding and the application of a Blackman window to reduce ringing.

## ASSOCIATED CONTENT

### Data Availability Statement

The data that support the findings of this study is available to download at the University of Cambridge's Apollo Repository [DOI to be added at acceptance].

### Supporting Information

The Supporting Information is available free of charge at https://pubs.acs.org/doi/10.1021/acsnano.5c08533.

Photoluminescence and Raman spectroscopy of mechanically exfoliated $WS_2$, additional analysis and discussion of impulsive vibrational spectroscopy data (PDF)

## AUTHOR INFORMATION


### Corresponding Author

**Akshay Rao** − *Department of Physics, Cavendish Laboratory, University of Cambridge, Cambridge CB3 0HE, U.K.;* orcid.org/0000-0003-4261-0766; Email: ar525@cam.ac.uk

### Authors

**Yorrick Boeije** − *Department of Chemical Engineering and Biotechnology, University of Cambridge, Cambridge CB3 0AS, U.K.; Department of Physics, Cavendish Laboratory, University of Cambridge, Cambridge CB3 0HE, U.K.;* orcid.org/0000-0002-4346-3123

**Anh Tuan Hoang** − *Department of Materials Science & Engineering, Stanford University, Stanford, California 94305, United States;* orcid.org/0000-0003-0911-1391

**Juhwan Lim** − *Department of Physics, Cavendish Laboratory, University of Cambridge, Cambridge CB3 0HE, U.K.; Department of Materials Science & Metallurgy, University of Cambridge, Cambridge CB3 0FS, U.K.*

**Samuel D. Stranks** − *Department of Chemical Engineering and Biotechnology, University of Cambridge, Cambridge CB3 0AS, U.K.; Department of Physics, Cavendish Laboratory, University of Cambridge, Cambridge CB3 0HE, U.K.;* orcid.org/0000-0002-8303-7292

**Manish Chhowalla** − *Department of Materials Science & Metallurgy, University of Cambridge, Cambridge CB3 0FS, U.K.;* orcid.org/0000-0002-8183-4044

**Eric Pop** − *Department of Materials Science & Engineering, Stanford University, Stanford, California 94305, United States; Department of Electrical Engineering and Department of Applied Physics, Stanford University, Stanford, California 94305, United States;* orcid.org/0000-0003-0436-8534

**Andrew J. Mannix** − *Department of Materials Science & Engineering, Stanford University, Stanford, California 94305, United States;* orcid.org/0000-0003-4788-1506

Complete contact information is available at: https://pubs.acs.org/10.1021/acsnano.5c08533


### Notes

The authors declare no competing financial interest.

## ACKNOWLEDGMENTS

Y.B. acknowledges the Winton Programme for Physics of Sustainability for funding. This project has received funding from the European Research Council under the European Union's Horizon 2020 research and innovation programme [Grant Agreement No. 758826 (SOLARX) to A.R.]. The authors thank Dr. Christoph Schnedermann, Dr. Takumi



https://doi.org/10.1021/acsnano.5c08533
ACS Nano 2025, 19, 26942−26952

Fukuda and Dr. Joshua Thompson for useful discussions. The Stanford authors acknowledge support from the US National Science Foundation FuSe2 Award No. 2425218, as well asTSMC through the Stanford SystemX alliance. For the purpose of open access, the authors have applied a Creative Commons Attribution (CC BY) license to any Author Accepted Manuscript version arising from this submission.

## REFERENCES

(1) Krenz, M.; Gerstmann, U.; Schmidt, W. G. Defect-Assisted Exciton Transfer across the Tetracene-Si(111):H Interface. *Phys. Rev. Lett.* **2024**, *132* (7), No. 076201.
(2) Pastor, E.; Sachs, M.; Selim, S.; Durrant, J. R.; Bakulin, A. A.; Walsh, A. Electronic Defects in Metal Oxide Photocatalysts. *Nat. Rev. Mater.* **2022**, *7* (7), 503−521.
(3) Stern, H. L.; Gu, Q.; Jarman, J.; Eizagirre Barker, S.; Mendelson, N.; Chugh, D.; Schott, S.; Tan, H. H.; Sirringhaus, H.; Aharonovich, I.; Atatüre, M. Room-Temperature Optically Detected Magnetic Resonance of Single Defects in Hexagonal Boron Nitride. *Nat. Commun.* **2022**, *13* (1), No. 618.
(4) Lim, J.; Lee, J. I.; Wang, Y.; Gauriot, N.; Sebastian, E.; Chhowalla, M.; Schnedermann, C.; Rao, A. Photoredox Phase Engineering of Transition Metal Dichalcogenides. *Nature* **2024**, *633* (8028), 83−89.
(5) Englund, D.; Shields, B.; Rivoire, K.; Hatami, F.; Vučković, J.; Park, H.; Lukin, M. D. Deterministic Coupling of a Single Nitrogen Vacancy Center to a Photonic Crystal Cavity. *Nano Lett.* **2010**, *10* (10), 3922−3926.
(6) Grosso, G.; Moon, H.; Lienhard, B.; Ali, S.; Efetov, D. K.; Furchi, M. M.; Jarillo-Herrero, P.; Ford, M. J.; Aharonovich, I.; Englund, D. Tunable and High-Purity Room Temperature Single-Photon Emission from Atomic Defects in Hexagonal Boron Nitride. *Nat. Commun.* **2017**, *8* (1), No. 705.
(7) Chakraborty, C.; Kinnischtzke, L.; Goodfellow, K. M.; Beams, R.; Vamivakas, A. N. Voltage-Controlled Quantum Light from an Atomically Thin Semiconductor. *Nat. Nanotechnol.* **2015**, *10* (6), 507−511.
(8) Rougieux, F. E.; Sun, C.; Macdonald, D. Determining the Charge States and Capture Mechanisms of Defects in Silicon through Accurate Recombination Analyses: A Review. *Sol. Energy Mater. Sol. Cells* **2018**, *187*, 263−272.
(9) Toyozawa, Y. Multiphonon Recombination Processes. *Solid-State Electron.* **1978**, *21* (11−12), 1313−1318.
(10) Whalley, L. D.; van Gerwen, P.; Frost, J. M.; Kim, S.; Hood, S. N.; Walsh, A. Giant Huang−Rhys Factor for Electron Capture by the Iodine Interstitial in Perovskite Solar Cells. *J. Am. Chem. Soc.* **2021**, *143* (24), 9123−9128.
(11) Barmparis, G. D.; Puzyrev, Y. S.; Zhang, X.-G.; Pantelides, S. T. Theory of Inelastic Multiphonon Scattering and Carrier Capture by Defects in Semiconductors: Application to Capture Cross Sections. *Phys. Rev. B* **2015**, *92*, No. 214111.
(12) Redfield, D.; Bube, R. H. *Photoinduced Defects in Semiconductors*; Cambridge University Press: Cambridge, 1996.
(13) Shi, L.; Wang, L.-W. Ab Initio Calculations of Deep-Level Carrier Nonradiative Recombination Rates in Bulk Semiconductors. *Phys. Rev. Lett.* **2012**, *109*, No. 245501.
(14) Stoneham, A. M. Non-Radiative Transitions in Semiconductors. *Rep. Prog. Phys.* **1981**, *44* (12), 1251.
(15) Henry, C. H.; Lang, D. V. Nonradiative Capture and Recombination by Multiphonon Emission in GaAs and GaP. *Phys. Rev. B* **1977**, *15* (2), 989−1016.
(16) Abumakov, V. N.; Perel, V. I.; Yassievich, I. N. *Nonradiative Recombination in Semiconductors*; Elsevier Science Publishers B.V: Amsterdam, 1991; Vol. *33*.
(17) Lengers, F.; Kuhn, T.; Reiter, D. E. Phonon-Mediated Exciton Capture in Mo-Based Transition Metal Dichalcogenides. *Phys. Rev. Res.* **2020**, *2* (4), No. 043160, DOI: 10.1103/PhysRevResearch.2.043160.
(18) Feierabend, M.; Brem, S.; Malic, E. Optical Fingerprint of Bright and Dark Localized Excitonic States in Atomically Thin 2D Materials. *Phys. Chem. Chem. Phys.* **2019**, *21* (47), 26077−26083.
(19) Cunningham, P. D.; McCreary, K. M.; Hanbicki, A. T.; Currie, M.; Jonker, B. T.; Hayden, L. M. Charge Trapping and Exciton Dynamics in Large-Area CVD Grown MoS2. *J. Phys. Chem. C* **2016**, *120* (10), 5819−5826.
(20) Handa, T.; Holbrook, M.; Olsen, N.; Holtzman, L. N.; Huber, L.; Wang, H. I.; Bonn, M.; Barmak, K.; Hone, J. C.; Pasupathy, A. N.; Zhu, X. Spontaneous Exciton Dissociation in Transition Metal Dichalcogenide Monolayers. *Sci. Adv.* **2024**, *10* (5), 31.
(21) Li, L.; Carter, E. A. Defect-Mediated Charge-Carrier Trapping and Nonradiative Recombination in WSe2Monolayers. *J. Am. Chem. Soc.* **2019**, *141* (26), 10451−10461.
(22) Gao, L.; Hu, Z.; Lu, J.; Liu, H.; Ni, Z. Defect-Related Dynamics of Photoexcited Carriers in 2D Transition Metal Dichalcogenides. *Phys. Chem. Chem. Phys.* **2021**, *23* (14), 8222−8235.
(23) Wang, H.; Zhang, C.; Rana, F. Ultrafast Dynamics of Defect-Assisted Electron-Hole Recombination in Monolayer MoS2. *Nano Lett.* **2015**, *15* (1), 339−345.
(24) An, H.; Li, J.; Liu, Y.; Xu, P.; Han, S.; Liu, Y.; Chen, S.; Li, S. Y.; Lin, C.; Pan, A. Tip-Enhanced Raman Spectroscopy of Monolayer MoS2 on Au(111). *J. Phys. Chem. C* **2024**, *128* (18), 7583−7590.
(25) Hase, M.; Kitajima, M. Interaction of Coherent Phonons with Defects and Elementary Excitations. *J. Phys.:Condens. Matter* **2010**, *22*, No. 073201.
(26) Hase, M.; Ishioka, K.; Kitajima, M.; Ushida, K.; Hishita, S. Dephasing of Coherent Phonons by Lattice Defects in Bismuth Films. *Appl. Phys. Lett.* **2000**, *76* (10), 1258−1260.
(27) Ichikawa, T.; Guo, J.; Fons, P.; Prananto, D.; An, T.; Hase, M. Cooperative Dynamic Polaronic Picture of Diamond Color Centers. *Nat. Commun.* **2024**, *15* (1), No. 7174.
(28) Keat, T. J.; Coxon, D. J. L.; Staniforth, M.; Dale, M. W.; Stavros, V. G.; Newton, M. E.; Lloyd-Hughes, J. Dephasing Dynamics across Different Local Vibrational Modes and Crystalline Environments. *Phys. Rev. Lett.* **2022**, *129* (23), No. 237401, DOI: 10.1103/PhysRevLett.129.237401.
(29) Liebel, M.; Schnedermann, C.; Wende, T.; Kukura, P. Principles and Applications of Broadband Impulsive Vibrational Spectroscopy. *J. Phys. Chem. A* **2015**, *119* (36), 9506−9517.
(30) Kuramochi, H.; Tahara, T. Tracking Ultrafast Structural Dynamics by Time-Domain Raman Spectroscopy. *J. Am. Chem. Soc.* **2021**, *143*, 9699−9717.
(31) Schnedermann, C.; Muders, V.; Ehrenberg, D.; Schlesinger, R.; Kukura, P.; Heberle, J. Vibronic Dynamics of the Ultrafast All-Trans to 13-Cis Photoisomerization of Retinal in Channelrhodopsin-1. *J. Am. Chem. Soc.* **2016**, *138* (14), 4757−4762.
(32) Ghosh, P.; Alvertis, A. M.; Chowdhury, R.; Murto, P.; Gillett, A. J.; Dong, S.; Sneyd, A. J.; Cho, H. H.; Evans, E. W.; Monserrat, B.; Li, F.; Schnedermann, C.; Bronstein, H.; Friend, R. H.; Rao, A. Decoupling Excitons from High-Frequency Vibrations in Organic Molecules. *Nature* **2024**, *629* (8011), 355−362.
(33) Batignani, G.; Fumero, G.; Srimath Kandada, A. R.; Cerullo, G.; Gandini, M.; Ferrante, C.; Petrozza, A.; Scopigno, T. Probing Femtosecond Lattice Displacement upon Photo-Carrier Generation in Lead Halide Perovskite. *Nat. Commun.* **2018**, *9* (1), No. 1971.
(34) Zhang, Z.; Hoang, L.; Hocking, M.; Peng, Z.; Hu, J.; Zaborski, G.; Reddy, P. D.; Dollard, J.; Goldhaber-Gordon, D.; Heinz, T. F.; Pop, E.; Mannix, A. J. Chemically Tailored Growth of 2D Semiconductors via Hybrid Metal-Organic Chemical Vapor Deposition. *ACS Nano* **2024**, *18*, 25414−25424.
(35) Zhu, Y.; Lim, J.; Zhang, Z.; Wang, Y.; Sarkar, S.; Ramsden, H.; Li, Y.; Yan, H.; Phuyal, D.; Gauriot, N.; Rao, A.; Hoye, R. L. Z.; Eda, G.; Chhowalla, M. Room-Temperature Photoluminescence Mediated by Sulfur Vacancies in 2D Molybdenum Disulfide. *ACS Nano* **2023**, *17*, 13545−13553.
(36) Bretscher, H.; Li, Z.; Xiao, J.; Qiu, D. Y.; Refaely-Abramson, S.; Alexander-Webber, J. A.; Tanoh, A.; Fan, Y.; Delport, G.; Williams, C. A.; Stranks, S. D.; Hofmann, S.; Neaton, J. B.; Louie, S. G.; Rao, A.

Rational Passivation of Sulfur Vacancy Defects in Two-Dimensional Transition Metal Dichalcogenides. *ACS Nano* **2021**, *15* (5), 8780−8789.
(37) Goodman, A. J.; Willard, A. P.; Tisdale, W. A. Exciton Trapping Is Responsible for the Long Apparent Lifetime in Acid-Treated MoS2. *Phys. Rev. B.* **2017**, *96* 12 DOI: 10.1103/PhysRevB.96.121404.
(38) Schuler, B.; Qiu, D. Y.; Refaely-Abramson, S.; Kastl, C.; Chen, C. T.; Barja, S.; Koch, R. J.; Ogletree, D. F.; Aloni, S.; Schwartzberg, A. M.; Neaton, J. B.; Louie, S. G.; Weber-Bargioni, A. Large Spin-Orbit Splitting of Deep In-Gap Defect States of Engineered Sulfur Vacancies in Monolayer WS 2. *Phys. Rev. Lett.* **2019**, *123*, No. 076801.
(39) Refaely-Abramson, S.; Qiu, D. Y.; Louie, S. G.; Neaton, J. B. Defect-Induced Modification of Low-Lying Excitons and Valley Selectivity in Monolayer Transition Metal Dichalcogenides. *Phys. Rev. Lett.* **2018**, *121*, No. 167402, DOI: 10.1103/PhysRevLett.121.167402.
(40) Barja, S.; Refaely-Abramson, S.; Schuler, B.; Qiu, D. Y.; Pulkin, A.; Wickenburg, S.; Ryu, H.; Ugeda, M. M.; Kastl, C.; Chen, C.; Hwang, C.; Schwartzberg, A.; Aloni, S.; Mo, S. K.; Frank Ogletree, D.; Crommie, M. F.; Yazyev, O. V.; Louie, S. G.; Neaton, J. B.; Weber-Bargioni, A. Identifying Substitutional Oxygen as a Prolific Point Defect in Monolayer Transition Metal Dichalcogenides. *Nat. Commun.* **2019**, *10* (1), No. 3382.
(41) Yang, J.; Wang, Y.; Lagos, M. J.; Manichev, V.; Fullon, R.; Song, X.; Voiry, D.; Chakraborty, S.; Zhang, W.; Batson, P. E.; Feldman, L.; Gustafsson, T.; Chhowalla, M. Single Atomic Vacancy Catalysis. *ACS Nano* **2019**, *13* (9), 9958−9964.
(42) Bianchi, M. G.; Risplendi, F.; Re Fiorentin, M.; Cicero, G. Engineering the Electrical and Optical Properties of WS2Monolayers via Defect Control. *Adv. Sci.* **2024**, *11* (4), No. 2305162.
(43) Liu, Y.; Cheng, X.; Wei, K.; Yang, H.; Jiang, T. Large Range Modification of Exciton Species in Monolayer $WS_2$. *Appl. Opt.* **2016**, *55* (23), 6251−6255.
(44) Berkdemir, A.; Gutiérrez, H. R.; Botello-Méndez, A. R.; Perea-López, N.; Elías, A. L.; Chia, C. I.; Wang, B.; Crespi, V. H.; López-Urías, F.; Charlier, J. C.; Terrones, H.; Terrones, M. Identification of Individual and Few Layers of WS2 Using Raman Spectroscopy. *Sci. Rep.* **2013**, *3* (1), No. 1755.
(45) Molina-Sánchez, A.; Wirtz, L. Phonons in Single-Layer and Few-Layer MoS2 and WS2. *Phys. Rev. B* **2011**, *84* (15), No. 155413, DOI: 10.1103/PhysRevB.84.155413.
(46) Li, Y.; Wu, X.; Liu, W.; Xu, H.; Liu, X. Revealing the Interrelation between C- And A-Exciton Dynamics in Monolayer WS2 via Transient Absorption Spectroscopy. *Appl. Phys. Lett.* **2021**, *119* (5), No. 051106, DOI: 10.1063/5.0060587/41422.
(47) Soni, A.; Kushavah, D.; Lu, L. S.; Chang, W. H.; Pal, S. K. Ultrafast Exciton Trapping and Exciton-Exciton Annihilation in Large-Area CVD-Grown Monolayer WS2. *J. Phys. Chem. C* **2021**, *125* (43), 23880−23888.
(48) Cunningham, P. D.; Hanbicki, A. T.; McCreary, K. M.; Jonker, B. T. Photoinduced Bandgap Renormalization and Exciton Binding Energy Reduction in WS2. *ACS Nano* **2017**, *11* (12), 12601−12608.
(49) Li, Y.; Wu, X.; Liu, W.; Xu, H.; Liu, X. Revealing the Interrelation between C- And A-Exciton Dynamics in Monolayer WS2 via Transient Absorption Spectroscopy. *Appl. Phys. Lett.* **2021**, *119* (5), No. 51106.
(50) Wang, Y.; Benny, A.; Le Dé, B.; Chin, A. W.; Scholes, G. D. A Numerically Exact Description of Ultrafast Vibrational Decoherence in Vibration-Coupled Electron Transfer. *Proc. Natl. Acad. Sci. U.S.A.* **2025**, *122* (9), No. e2416542122.
(51) Takeuchi, E.; Muramatsu, M.; Yoneda, Y.; Katayama, T.; Iwamoto, A.; Nagasawa, Y.; Miyasaka, H. Vibrational Decoherence Induced by Ultrafast Intramolecular Charge Separation of an Asymmetric Bianthryl Derivative. *J. Chem. Phys.* **2020**, *153* (8), No. 84307.
(52) Rafiq, S.; Scholes, G. D. Is Back-Electron Transfer Process in Betaine-30 Coherent? *Chem. Phys. Lett.* **2017**, *683*, 500−506.
(53) Freixas, V. M.; Keefer, D.; Tretiak, S.; Fernandez-Alberti, S.; Mukamel, S. Ultrafast Coherent Photoexcited Dynamics in a Trimeric Dendrimer Probed by X-Ray Stimulated-Raman Signals. *Chem. Sci.* **2022**, *13* (21), 6373−6384.
(54) Srivastava, G. P.; Thomas, I. O. Temperature-Dependent Raman Linewidths in Transition-Metal Dichalcogenides. *Phys. Rev. B* **2018**, *98*, No. 35430.
(55) Trovatello, C.; Miranda, H. P. C.; Molina-Sánchez, A.; Borrego-Varillas, R.; Manzoni, C.; Moretti, L.; Ganzer, L.; Maiuri, M.; Wang, J.; Dumcenco, D.; Kis, A.; Wirtz, L.; Marini, A.; Soavi, G.; Ferrari, A. C.; Cerullo, G.; Sangalli, D.; Conte, S. D. Strongly Coupled Coherent Phonons in Single-Layer MoS2. *ACS Nano* **2020**, *14* (5), 5700−5710.
(56) Jeong, T. Y.; Jin, B. M.; Rhim, S. H.; Debbichi, L.; Park, J.; Jang, Y. D.; Lee, H. R.; Chae, D. H.; Lee, D.; Kim, Y. H.; Jung, S.; Yee, K. J. Coherent Lattice Vibrations in Mono- and Few-Layer WSe2. *ACS Nano* **2016**, *10* (5), 5560−5566.
(57) Attar, A. R.; Chang, H. T.; Britz, A.; Zhang, X.; Lin, M. F.; Krishnamoorthy, A.; Linker, T.; Fritz, D.; Neumark, D. M.; Kalia, R. K.; Nakano, A.; Ajayan, P.; Vashishta, P.; Bergmann, U.; Leone, S. R. Simultaneous Observation of Carrier-Specific Redistribution and Coherent Lattice Dynamics in 2H-MoTe2 with Femtosecond Core-Level Spectroscopy. *ACS Nano* **2020**, *14* (11), 15829−15840.
(58) Gu, X.; Yang, R. Phonon Transport in Single-Layer Transition Metal Dichalcogenides: A First-Principles Study. *Appl. Phys. Lett.* **2014**, *105* (13), No. 131903.
(59) Han, S.; Boguschewski, C.; Gao, Y.; Xiao, L.; Zhu, J.; Van Loosdrecht, P. H. M. Incoherent Phonon Population and Exciton-Exciton Annihilation in Monolayer WS2 Revealed by Time-Resolved Spontaneous Raman Scattering. *Opt. Express* **2019**, *27* (21), 29949−29961.
(60) Cai, Y.; Lan, J.; Zhang, G.; Zhang, Y.-W. Lattice Vibrational Modes and Phonon Thermal Conductivity of Monolayer MoS 2. *Phys. Rev. B* **2014**, *89*, No. 35438.
(61) Li, J. J.; Chen, J.; Reis, D. A.; Fahy, S.; Merlin, R. Optical Probing of Ultrafast Electronic Decay in Bi and Sb with Slow Phonons. *Phys. Rev. Lett.* **2013**, *110*, No. 047401.
(62) Fukuda, T.; Makino, K.; Saito, Y.; Fons, P.; Ando, A.; Mori, T.; Ishikawa, R.; Ueno, K.; Afalla, J.; Hase, M. Coherent Optical Response Driven by Non-Equilibrium Electron-Phonon Dynamics in a Layered Transition-Metal Dichalcogenide. *APL Mater.* **2024**, *12* (2), No. 021102, DOI: 10.1063/5.0188537.
(63) Zou, J.; Zhu, R.; Wang, J.; Meng, H.; Wang, Z.; Chen, H.; Weng, Y. X. Coherent Phonon-Mediated Many-Body Interaction in Monolayer WSe2. *J. Phys. Chem. Lett.* **2023**, *14* (20), 4657−4665.
(64) Sun, L.; Kumar, P.; Liu, Z.; Choi, J.; Fang, B.; Roesch, S.; Tran, K.; Casara, J.; Priego, E.; Chang, Y. M.; Moody, G.; Silverman, K. L.; Lorenz, V. O.; Scheibner, M.; Luo, T.; Li, X. Phonon Dephasing Dynamics in MoS2. *Nano Lett.* **2021**, *21* (3), 1434−1439.
(65) Kühl, A.; Domcke, W. Multilevel Redfield Description of the Dissipative Dynamics at Conical Intersections. *J. Chem. Phys.* **2002**, *116* (1), 263−274.
(66) Rather, S.; Fu, B.; Kudisch, B.; Scholes, G. D. Interplay of Vibrational Wavepackets during an Ultrafast Electron Transfer Reaction. *Nat. Chem.* **2020**, *13* (1), 70−77.
(67) Rather, S. R.; Weingartz, N. P.; Kromer, S.; Castellano, F. N.; Chen, L. X. Spin−Vibronic Coherence Drives Singlet−Triplet Conversion. *Nature* **2023**, *620* (7975), 776−781.
(68) Yoneda, Y.; Kudisch, B.; Rafiq, S.; Maiuri, M.; Nagasawa, Y.; Scholes, G. D.; Miyasaka, H. Vibrational Dephasing along the Reaction Coordinate of an Electron Transfer Reaction. *J. Am. Chem. Soc.* **2021**, *143* (36), 14511−14522.
(69) Paulus, B. C.; Adelman, S. L.; Jamula, L. L.; McCusker, J. K. Leveraging Excited-State Coherence for Synthetic Control of Ultrafast Dynamics. *Nature* **2020**, *582*, 214−219.
(70) Man, M. K. L.; Madéo, J.; Sahoo, C.; Xie, K.; Campbell, M.; Pareek, V.; Karmakar, A.; Wong, E. L.; Al-Mahboob, A.; Chan, N. S.; Bacon, D. R.; Zhu, X.; Abdelrasoul, M. M. M.; Li, X.; Heinz, T. F.; Da Jornada, F. H.; Cao, T.; Dani, K. M. Experimental Measurement Ofthe Intrinsic Excitonic Wave Function. *Sci. Adv.* **2021**, *7* (17), 192−213.

(71) Bae, S.; Jeong, Y. T.; Raebiger, H.; Yee, K.-J.; Kim, Y.-H. Localized Coherent Phonon Generation in Monolayer MoSe2 from Ultrafast Exciton Trapping at Shallow Traps. *Nanoscale Horiz.* **2023**, *8*, 1282−1287, DOI: 10.1039/D3NH00194F.
(72) Huang, K.; Rhys, A. Theory of Light Absorption and Non-Radiative Transitions in F-Centres. *Proc. R. Soc. London, Ser. A* **1950**, *204* (1078), 406−423.
(73) Pyosang, K.; Subhangi, R.; Valentine, A. J.; Xiaolin, L.; Sarah, K.; Kim, T. W.; Xiaosong, L.; Castellano, F. N.; Chen, L. X. Real-Time Capture of Nuclear Motions Influencing Photoinduced Electron Transfer. *Chem. Sci.* **2024**, *15*, 14766−14777, DOI: 10.1039/D4SC01876A.
(74) Schnedermann, C.; Liebel, M.; Kukura, P. Mode-Specificity of Vibrationally Coherent Internal Conversion in Rhodopsin during the Primary Visual Event. *J. Am. Chem. Soc.* **2015**, *137* (8), 2886−2891.
(75) Ghosh, I.; Shen, Q.; Wu, P. J. E.; Engel, G. S. Vibronic Conical Intersection Trajectory Signatures in Wave Packet Coherences. *J. Phys. Chem. Lett.* **2024**, *15*, 12494−12500.
(76) Schnedermann, C.; Alvertis, A. M.; Wende, T.; Lukman, S.; Feng, J.; Schröder, F. A. Y. N.; Turban, D. H. P.; Wu, J.; Hine, N. D. M.; Greenham, N. C.; Chin, A. W.; Rao, A.; Kukura, P.; Musser, A. J. A Molecular Movie of Ultrafast Singlet Fission. *Nat. Commun.* **2019**, *10* (1), No. 4207.
(77) Hetherington, C. V.; Mohan, T. M. N.; Tilluck, R. W.; Beck, W. F.; Levine, B. G. Origin of Vibronic Coherences During Carrier Cooling in Colloidal Quantum Dots. *J. Phys. Chem. Lett.* **2023**, *14* (51), 11651−11658.
(78) Liebel, M.; Schnedermann, C.; Kukura, P. Vibrationally Coherent Crossing and Coupling of Electronic States during Internal Conversion in $\beta$-Carotene. *Phys. Rev. Lett.* **2014**, *112* (19), No. 198302, DOI: 10.1103/PhysRevLett.112.198302.
(79) Boeije, Y.; Olivucci, M. From a One-Mode to a Multi-Mode Understanding of Conical Intersection Mediated Ultrafast Organic Photochemical Reactions. *Chem. Soc. Rev.* **2023**, *52* (8), 2643−2687.
(80) Keefer, D.; Freixas, V. M.; Song, H.; Tretiak, S.; Fernandez-Alberti, S.; Mukamel, S. Monitoring Molecular Vibronic Coherences in a Bichromophoric Molecule by Ultrafast X-Ray Spectroscopy. *Chem. Sci.* **2021**, *12* (14), 5286−5294.
(81) Stern, H. L.; Cheminal, A.; Yost, S. R.; Broch, K.; Bayliss, S. L.; Chen, K.; Tabachnyk, M.; Thorley, K.; Greenham, N.; Hodgkiss, J. M.; Anthony, J.; Head-Gordon, M.; Musser, A. J.; Rao, A.; Friend, R. H. Vibronically Coherent Ultrafast Triplet-Pair Formation and Subsequent Thermally Activated Dissociation Control Efficient Endothermic Singlet Fission. *Nat. Chem.* **2017**, *9*, 1205−1212.
(82) Wang, Q.; Schoenlein, R. W.; Peteanu, L. A.; Mathies, R. A.; Shank, C. V. Vibrationally Coherent Photochemistry in the Femtosecond Primary Event of Vision. *Science* **1994**, *266* (5184), 422−424.
(83) Liebel, M.; Schnedermann, C.; Bassolino, G.; Taylor, G.; Watts, A.; Kukura, P. Direct Observation of the Coherent Nuclear Response after the Absorption of a Photon. *Phys. Rev. Lett.* **2014**, *112*, No. 238301.
(84) Kumar, A. T. N.; Rosca, F.; Widom, A.; Champion, P. M. Investigations of Amplitude and Phase Excitation Profiles in Femtosecond Coherence Spectroscopy. *J. Chem. Phys.* **2001**, *114* (2), 701−724.
(85) Jean, J. M.; Fleming, G. R. Competition between Energy and Phase Relaxation in Electronic Curve Crossing Processes. *J. Chem. Phys.* **1995**, *103*, 2092−2101.
(86) Van Der Veen, R. M.; Cannizzo, A.; Van Mourik, F.; Vlček, A.; Chergui, M. Vibrational Relaxation and Intersystem Crossing of Binuclear Metal Complexes in Solution. *J. Am. Chem. Soc.* **2011**, *133* (2), 305−315.
(87) Dexheimer, S. L.; Van Pelt, A. D.; Brozik, J. A.; Swanson, B. I. Femtosecond Vibrational Dynamics of Self-Trapping in a Quasi-One-Dimensional System. *Phys. Rev. Lett.* **2000**, *84* (19), 4425−4428.
(88) Califano, S.; Schettino, V. Vibrational Relaxation in Molecular Crystals. *Int. Rev. Phys. Chem.* **1988**, *7* (1), 19−57.
(89) Cortecchia, D.; Yin, J.; Petrozza, A.; Soci, C. White Light Emission in Low-Dimensional Perovskites. *J. Mater. Chem. C* **2019**, *7* (17), 4956−4969.
(90) Li, S.; Luo, J.; Liu, J.; Tang, J. Self-Trapped Excitons in All-Inorganic Halide Perovskites: Fundamentals, Status, and Potential Applications. *J. Phys. Chem. Lett.* **2019**, *10* (8), 1999−2007.
(91) Onuchic, J. N.; Wolynes, P. G. Classical and Quantum Pictures of Reaction Dynamics in Condensed Matter: Resonances, Dephasing, and All That. *J. Phys. Chem. A* **1988**, *92*, 6495−6503.
(92) Musser, A. J.; Liebel, M.; Schnedermann, C.; Wende, T.; Kehoe, T. B.; Rao, A.; Kukura, P. Evidence for Conical Intersection Dynamics Mediating Ultrafast Singlet Exciton Fission. *Nat. Phys.* **2015**, *11* (4), 352−357.
(93) Rather, S. R.; Scholes, G. D. From Fundamental Theories to Quantum Coherences in Electron Transfer. *J. Am. Chem. Soc.* **2019**, *141* (2), 708−722.
(94) Kambhampati, P.; Son, D. H.; Kee, T. W.; Barbara, P. F. Solvent Effects on Vibrational Coherence and Ultrafast Reaction Dynamics in the Multicolor Pump-Probe Spectroscopy of Intervalence Electron Transfer. *J. Phys. Chem. A* **2000**, *104* (46), 10637−10644.
(95) Pollard, W. T.; Dexheimer, S. L.; Wang, J.-Q.; Peteanu, J.-L. A.; Shank, C. V.; Mathies, R. A. Theory of Dynamic Absorption Spectroscopy of Nonstationary States. 4. Application to 12-Fs Resonant Impulsive Raman Spectroscopy of Bacteriorhodopsin. *J. Phys. Chem. A* **1992**, *96*, 6147−6158.
(96) Zeiger, H. J.; Vidal, J.; Cheng, T. K.; Ippen, E. P.; Dresselhaus, G.; Dresselhaus, M. S. Theory for Displacive Excitation of Coherent Phonons. *Phys. Rev. B* **1992**, *45* (2), 768−778.
(97) Garrett, G. A.; Albrecht, T. F.; Whitaker, J. F.; Merlin, R. Coherent THz Phonons Driven by Light Pulses and the Sb Problem: What Is the Mechanism? *Phys. Rev. Lett.* **1996**, *77*, No. 3661.
(98) Stevens, T. E.; Kuhl, J.; Merlin, R. Coherent Phonon Generation and the Two Stimulated Raman Tensors. *Phys. Rev. B* **2002**, *65* (14), No. 144304.
(99) Riffe, D. M.; Sabbah, A. J. Coherent Excitation of the Optic Phonon in Si: Transiently Stimulated Raman Scattering with a Finite-Lifetime Electronic Excitation. *Phys. Rev. B* **2007**, *76* (8), No. 085207, DOI: 10.1103/PhysRevB.76.085207.
(100) Shu, Y.; Fales, B. S.; Levine, B. G. Defect-Induced Conical Intersections Promote Nonradiative Recombination. *Nano Lett.* **2015**, *15* (9), 6247−6253.
(101) Levine, B. G.; Esch, M. P.; Fales, B. S.; Hardwick, D. T.; Peng, W.-T.; Shu, Y. Conical Intersections at the Nanoscale: Molecular Ideas for Materials. *Annu. Rev. Phys. Chem.* **2019**, *70* (1), 21−43.
(102) Bozyigit, D.; Yazdani, N.; Yarema, M.; Yarema, O.; Lin, W. M. M.; Volk, S.; Vuttivorakulchai, K.; Luisier, M.; Juranyi, F.; Wood, V. Soft Surfaces of Nanomaterials Enable Strong Phonon Interactions. *Nature* **2016**, *531* (7596), 618−622.
(103) Sykes, M. E.; Kim, M.; Wu, X.; Wiederrecht, G. P.; Peng, L.; Wang, Y. H.; Gosztola, D. J.; Ma, X. Ultrafast Exciton Trapping at Sp3 Quantum Defects in Carbon Nanotubes. *ACS Nano* **2019**, *13* (11), 13264−13270.
(104) Doherty, T. A. S.; Winchester, A. J.; Macpherson, S.; Johnstone, D. N.; Pareek, V.; Tennyson, E. M.; Kosar, S.; Kosasih, F. U.; Anaya, M.; Abdi-Jalebi, M.; Andaji-Garmaroudi, Z.; Wong, E. L.; Madéo, J.; Chiang, Y.-H.; Park, J.-S.; Jung, Y.-K.; Petoukhoff, C. E.; Divitini, G.; Man, M. K. L.; Ducati, C.; Walsh, A.; Midgley, P. A.; Dani, K. M.; Stranks, S. D. Performance-Limiting Nanoscale Trap Clusters at Grain Junctions in Halide Perovskites. *Nature* **2020**, *580* (7803), 360−366.
(105) Guzelturk, B.; Cotts, B. L.; Jasrasaria, D.; Philbin, J. P.; Hanifi, D. A.; Koscher, B. A.; Balan, A. D.; Curling, E.; Zajac, M.; Park, S.; Yazdani, N.; Nyby, C.; Kamysbayev, V.; Fischer, S.; Nett, Z.; Shen, X.; Kozina, M. E.; Lin, M. F.; Reid, A. H.; Weathersby, S. P.; Schaller, R. D.; Wood, V.; Wang, X.; Dionne, J. A.; Talapin, D. V.; Alivisatos, A. P.; Salleo, A.; Rabani, E.; Lindenberg, A. M. Dynamic Lattice Distortions Driven by Surface Trapping in Semiconductor Nanocrystals. *Nat. Commun.* **2021**, *12* (1), No. 1860.

(106) Saari, J. I.; Dias, E. A.; Reifsnyder, D.; Krause, M. M.; Walsh, B. R.; Murray, C. B.; Kambhampati, P. Ultrafast Electron Trapping at the Surface of Semiconductor Nanocrystals: Excitonic and Biexcitonic Processes. *J. Phys. Chem. B* **2013**, *117* (16), 4412−4421.
(107) Li, W.; Liu, J.; Bai, F.-Q.; Zhang, H.-X.; Prezhdo, O. V. Hole Trapping by Iodine Interstitial Defects Decreases Free Carrier Losses in Perovskite Solar Cells: A Time-Domain Ab Initio Study. *ACS Energy Lett.* **2017**, *2* (6), 1270−1278.
(108) Schmitt, D.; Bange, J. P.; Bennecke, W.; AlMutairi, A. A.; Meneghini, G.; Watanabe, K.; Taniguchi, T.; Steil, D.; Luke, D. R.; Weitz, R. T.; Steil, S.; Jansen, G. S. M.; Brem, S.; Malic, E.; Hofmann, S.; Reutzel, M.; Mathias, S. Formation of Moiré Interlayer Excitons in Space and Time. *Nature* **2022**, *608* (7923), 499−503.
(109) Perea-Causín, R.; Brem, S.; Malic, E. Phonon-Assisted Exciton Dissociation in Transition Metal Dichalcogenides. *Nanoscale* **2021**, *13* (3), 1884−1892.
(110) Brem, S.; Ekman, A.; Christiansen, D.; Katsch, F.; Selig, M.; Robert, C.; Marie, X.; Urbaszek, B.; Knorr, A.; Malic, E. Phonon-Assisted Photoluminescence from Indirect Excitons in Monolayers of Transition-Metal Dichalcogenides. *Nano Lett.* **2020**, *20* (4), 2849−2856.
(111) Tyagi, P.; Cooney, R. R.; Sewall, S. L.; Sagar, D. M.; Saari, J. I.; Kambhampati, P. Controlling Piezoelectric Response in Semiconductor Quantum Dots via Impulsive Charge Localization. *Nano Lett.* **2010**, *10* (8), 3062−3067.
(112) Sie, E. J.; Steinhoff, A.; Gies, C.; Lui, C. H.; Ma, Q.; Rösner, M.; Schönhoff, G.; Jahnke, F.; Wehling, T. O.; Lee, Y. H.; Kong, J.; Jarillo-Herrero, P.; Gedik, N. Observation of Exciton Redshift-Blueshift Crossover in Monolayer WS2. *Nano Lett.* **2017**, *17* (7), 4210−4216.





https://doi.org/10.1021/acsnano.5c08533
*ACS Nano* 2025, 19, 26942−26952

# Supporting Information

## Vibronically coherent exciton trapping in monolayer $WS_2$

**Authors:** Yorrick Boeije[1,2], Anh Tuan Hoang[3], Juhwan Lim[2,4], Samuel D. Stranks[1,2], Manish Chhowalla[4], Eric Pop[3,5,6], Andrew J Mannix[3], Akshay Rao[2]*

**Affiliations:**

[1]Department of Chemical Engineering and Biotechnology, University of Cambridge; Cambridge, UK.

[2]Department of Physics, Cavendish Laboratory, University of Cambridge; Cambridge, UK.

[3]Department of Materials Science & Engineering, Stanford University, Stanford, California 94305, United States.

[4]Department of Materials Science & Metallurgy, University of Cambridge; Cambridge, UK.

[5]Department of Electrical Engineering, Stanford University, Stanford, California 94305, United States.

[6]Department of Applied Physics, Stanford University, Stanford, California 94305, United States.

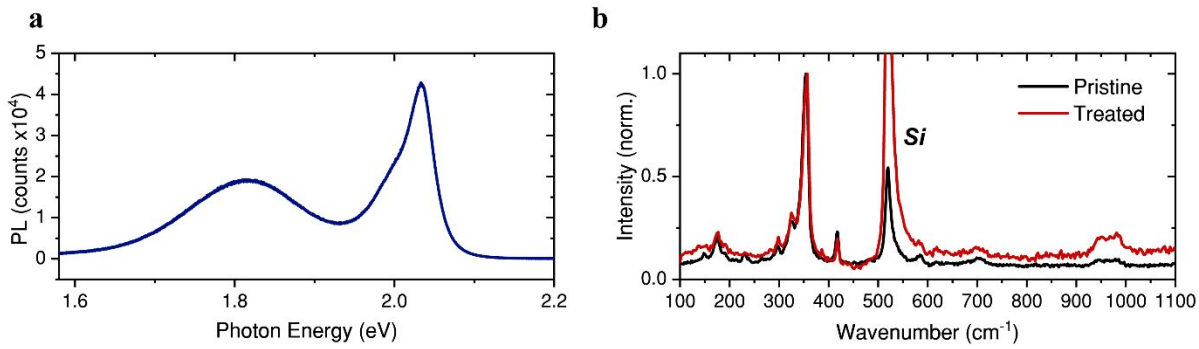


**Supplementary Figure S1**. (a) Room temperature photoluminescence spectrum ($\lambda_{exc}$ = 532 nm) of a *n*Bu-Li treated monolayer $WS_2$ prepared with mechanical exfoliation. (b) Raman spectra of treated and untreated films. The silicon peak is indicated.

**Supplementary Note 1**

We assign the 419 $cm^{-1}$ mode to A', despite its proximity to a sapphire mode, based on the clear nodal pattern in the Raman map, emphasizing its coupling to excitonic transitions (as is also observed for E') (Fig. S2). In contrast, the sapphire mode is insensitive to probe wavelength as it is probed off-resonantly (Fig. S3).[1] Furthermore, other sapphire modes (576 $cm^{-1}$ and 750 $cm^{-1}$) do not appear in the $WS_2$ fast Fourier transform (FFT) spectra. Upon edge excitation of the $WS_2$ monolayer (Fig. S4), the disappearance of the 419 $cm^{-1}$ nodal pattern, the absence of any E' mode and appearance of the other sapphire modes suggest that the off-resonant impulsive stimulated Raman scattering (ISRS) mechanism dominates for this excitation condition. In contrast, the appearance of A' and E' modes for on-resonant excitation of $WS_2$ (Fig. S2) suggests that these modes are generated via resonant-ISRS or via the displacive excitation of coherent phonons (DECP) mechanism.[2,3] The spectral π-phase flip of both A' and E' modes present when $WS_2$ is excited on-resonantly, supports their excited state nature, as ground state wavepackets generated by the off-resonant ISRS mechanism have no π-phase flip (Fig. S8).[4]

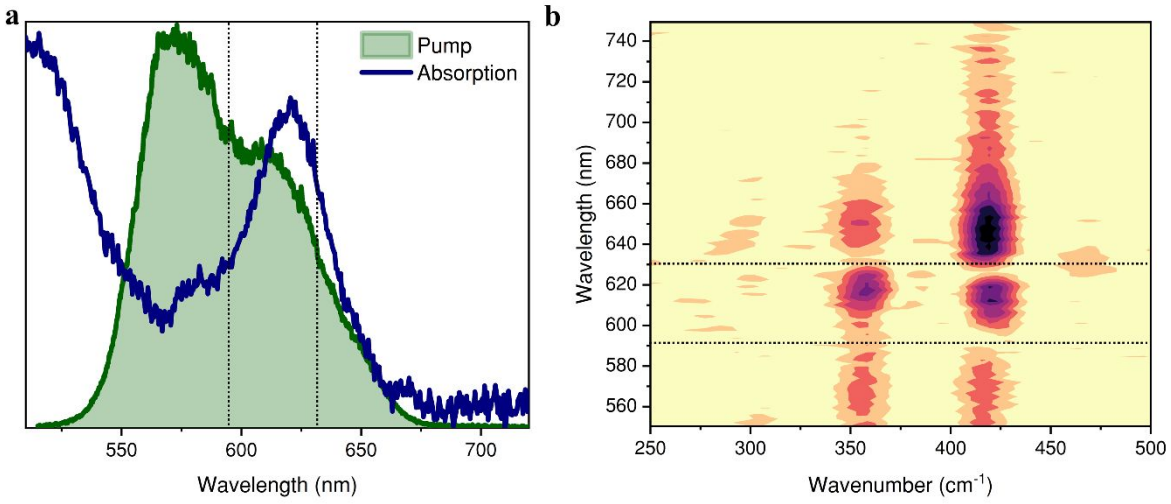


**Figure S2**. (a) Green broadband pump and absorption spectrum. (b) Room temperature ultrafast Raman map of *n*Bu-Li treated $WS_2$ film. The two nodes are marked with a dotted black line, and also indicated in the absorption spectrum.

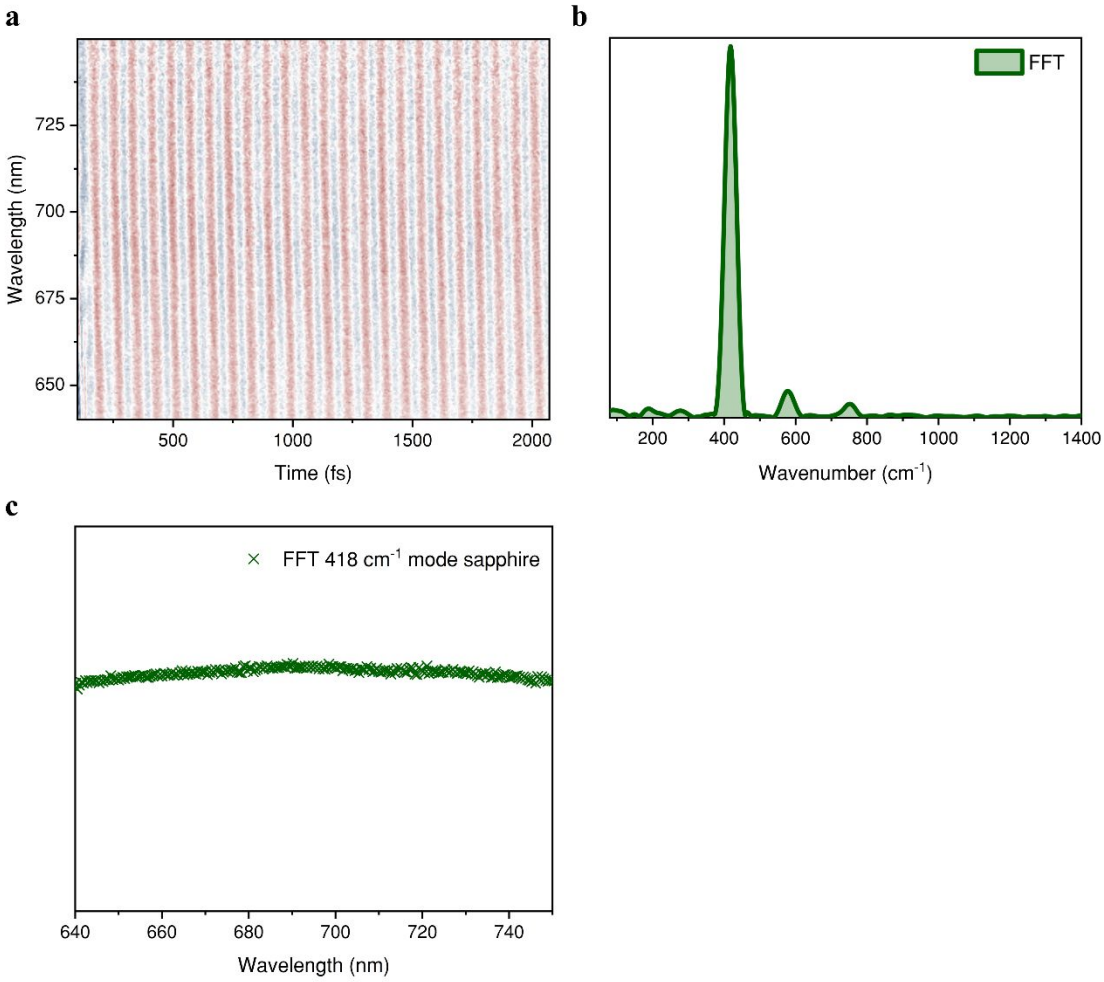


**Figure S3**. (a) Transient absorption map of sapphire substrate pumped with same broadband pulse as shown in Fig. S2a. (b) The FFT spectrum of the 670-720 nm probe region. (c) FFT intensity dependence on probe wavelength of 418 $cm^{-1}$ mode.

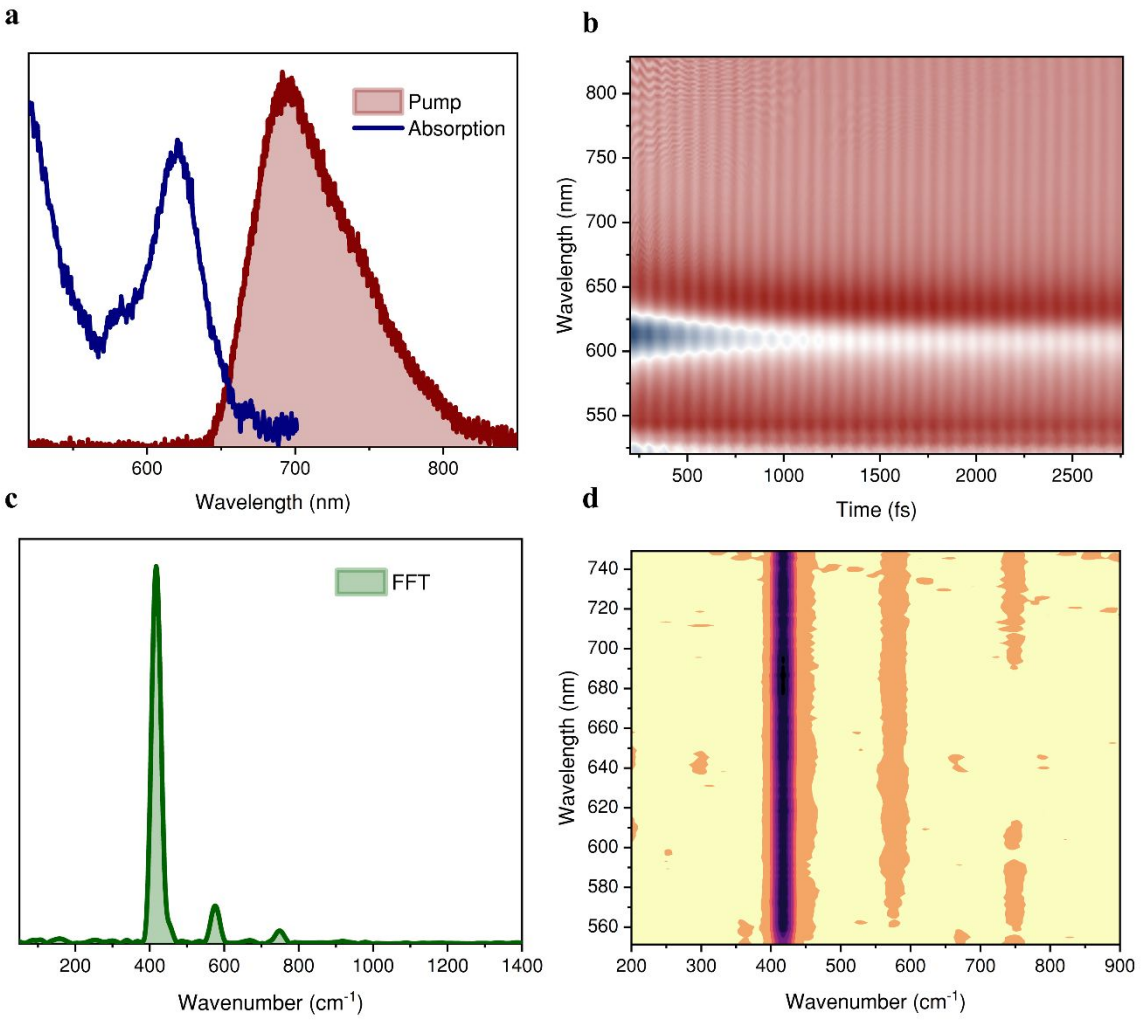


**Figure S4**. (a) Red broadband pump and absorption spectrum. (b) Transient absorption map of *n*Bu-Li treated $WS_2$ film. (c) The FFT spectrum of the 670-720 nm spectral region. (d) FFT map.

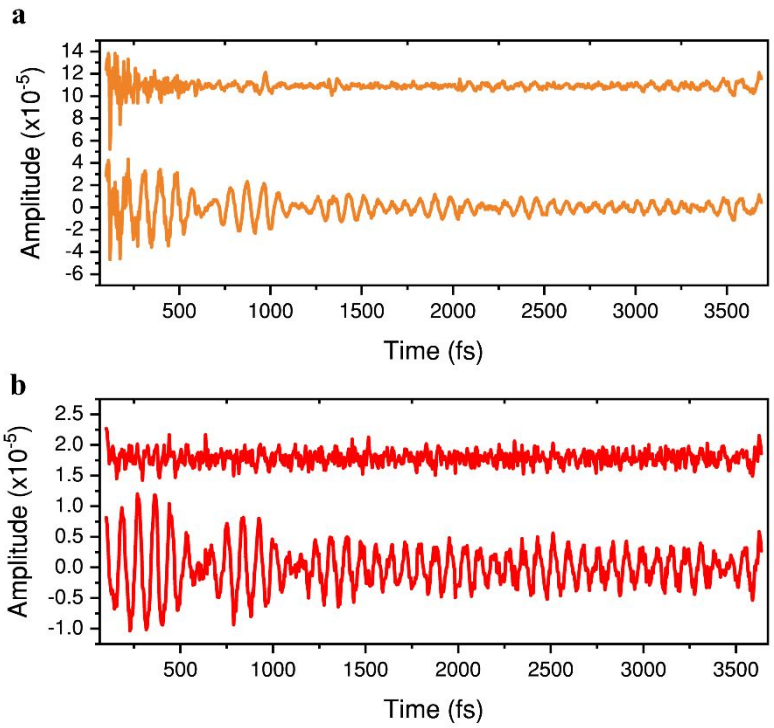


**Figure S5**. (a) Residuals overlaid on the electronic decay-free transient of the free exciton. (b) Residuals overlaid on the electronic decay-free transient of the trapped exciton. (The original transients are also shown in Fig. 3c and 3d of the main text.)

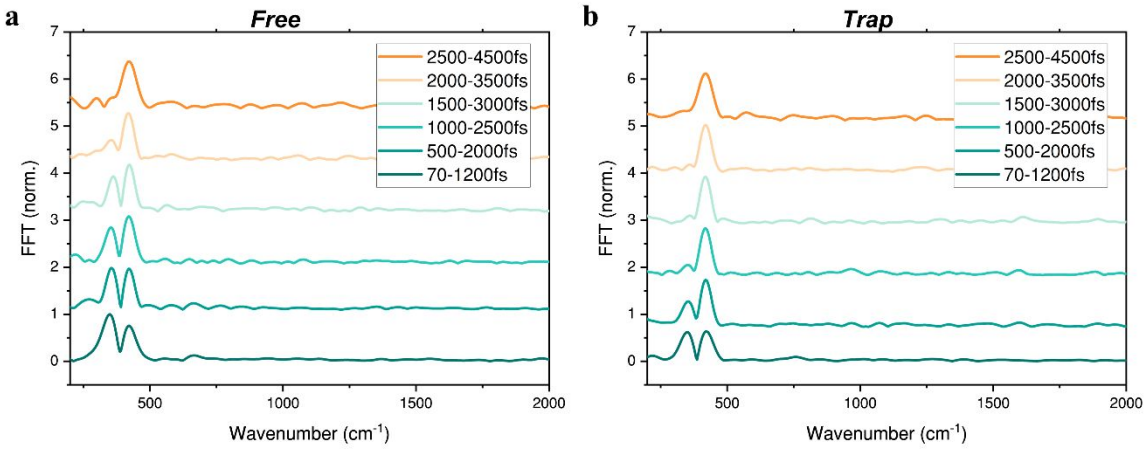


**Figure S6**. (a) Sliding-window FFT for free exciton. (b) Sliding-window FFT for trapped exciton.

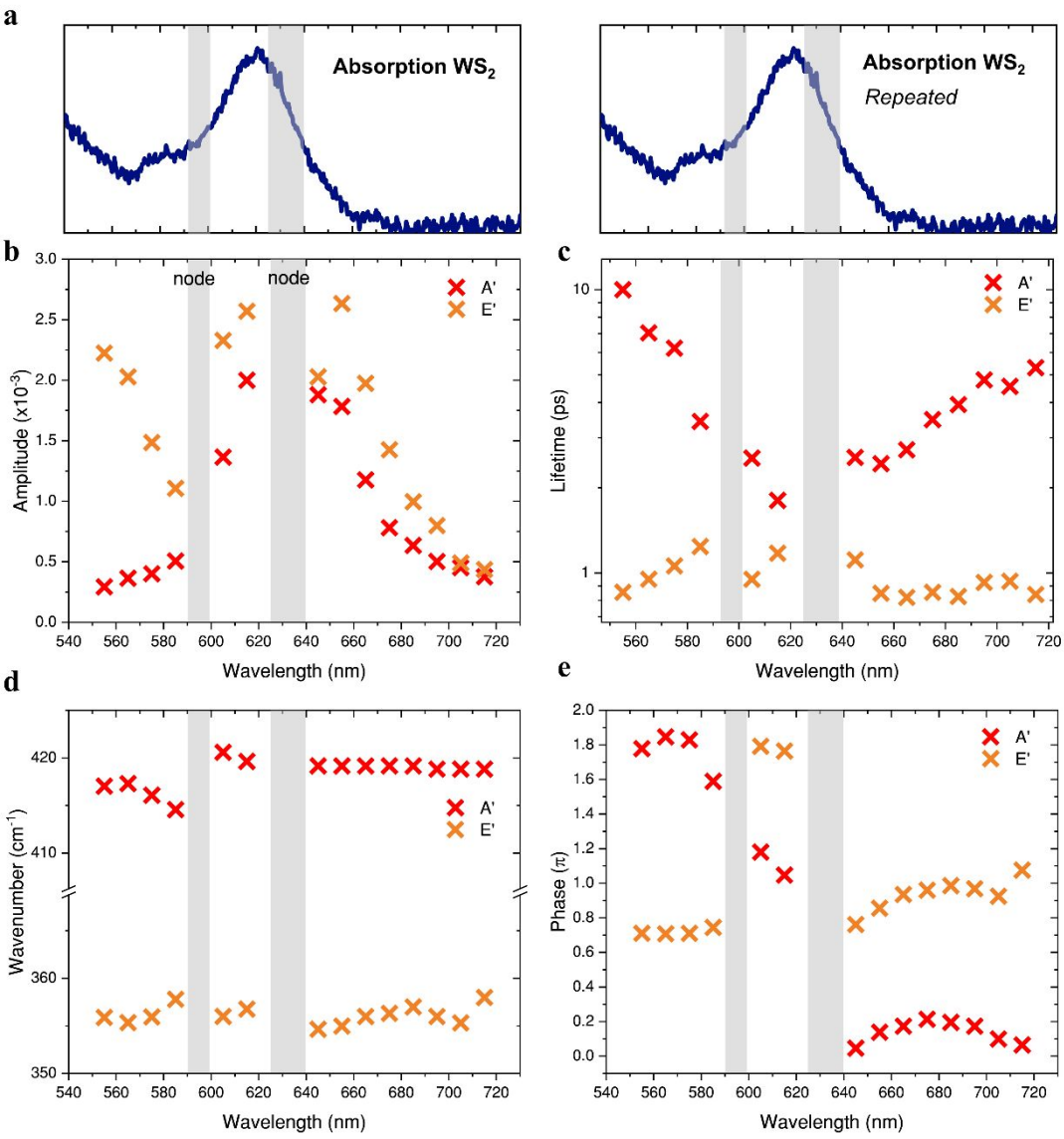


**Figure S7**. Spectral-dependence of damped sinusoid fitting. (a) Nodal spectral regions are indicated with grey boxes and are aligned with the absorption spectrum of $WS_2$. (b) Spectral dependence of amplitude. (c) Spectral dependence of lifetime. (d) Spectral dependence of wavenumber. (e) Spectral dependence of phase. Representative oscillatory traces are provided in Fig. S5.

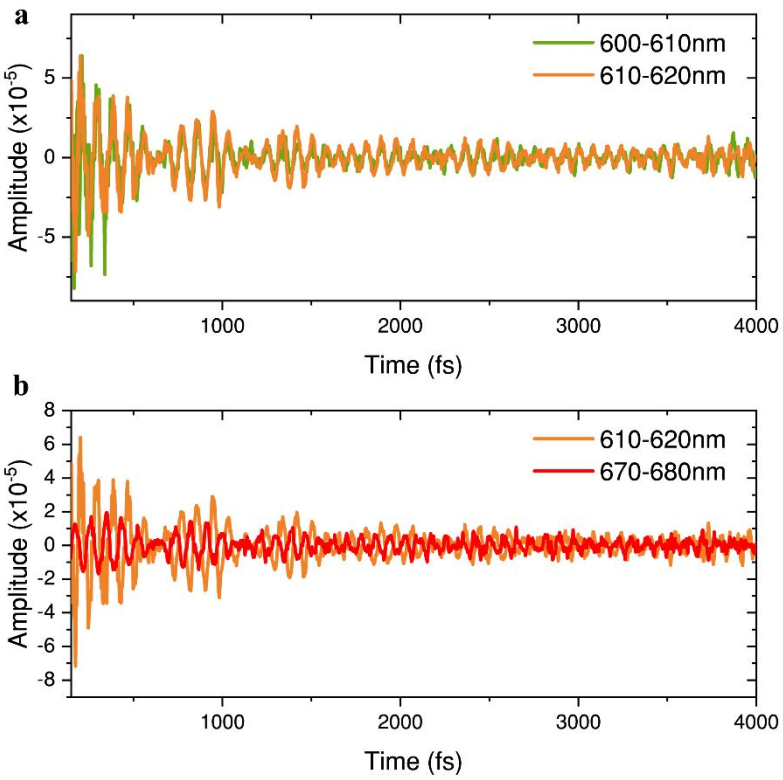


**Figure S8**. (a) In-phase oscillatory traces for two spectral slices of exciton A. (b) Oscillatory traces between exciton A and trapped exciton show out-of-phase relationship.

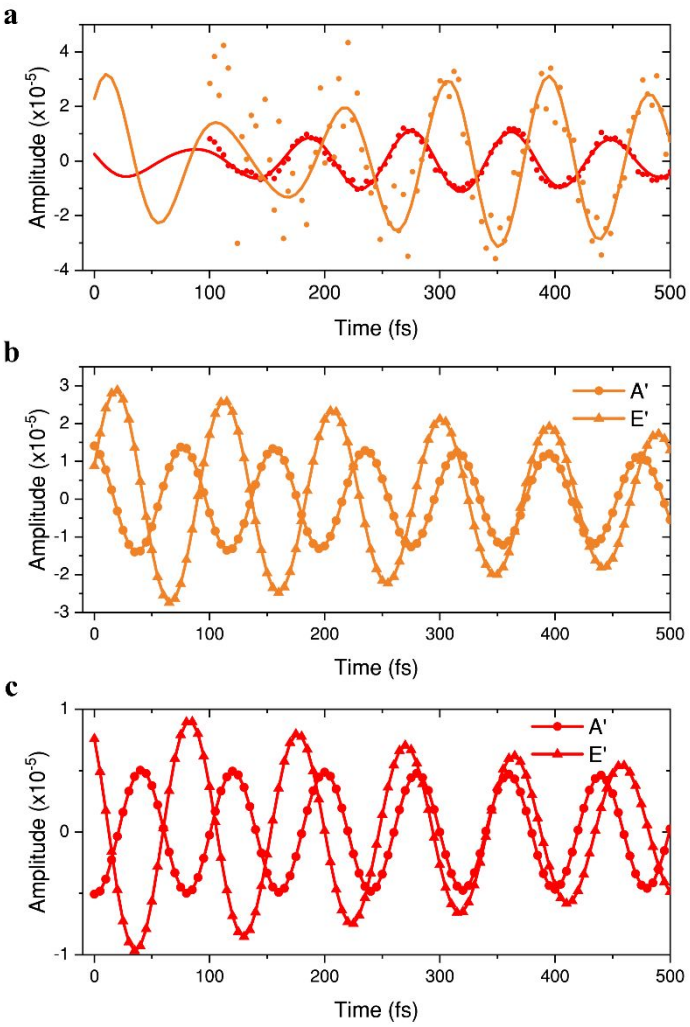


**Figure S9**. (a) Oscillatory traces of free (600-625 nm, orange) and trapped (670-720 nm, red) excitons (Fig. 3c and 3d in the main text) and their extrapolated damped sinusoid fits to $t = 0$ fs. Fitted parameters are provided in Table 1 of the main text. (b) Mode-specific extrapolated fits for free exciton. (c) Mode-specific extrapolated fits for trapped exciton.

**Supplementary Note 2**

Ignoring defect-induced symmetry breaking, a group theory based argument can be made using the $C_{3h}$ point group at the K band edge.[5] As the valence band maximum and conduction band minimum at the K point have E' and A' symmetry, respectively, the in-plane exciton has E' symmetry. Assuming the trapped exciton retains the same symmetry, the non-adiabatic coupling matrix element $\left\langle \varphi_{trapped} \left| \frac{\partial}{\partial Q} \right| \varphi_{free} \right\rangle$ is non-zero as the direct product E' ⊗ E' ⊗ E' contains the totally symmetric irreducible representation of $C_{3h}$, $A_1$'.

## References

(1) Liebel, M.; Schnedermann, C.; Wende, T.; Kukura, P. Principles and Applications of Broadband Impulsive Vibrational Spectroscopy. *J. Phys. Chem. A* **2015**, *119* (36), 9506–9517. DOI:10.1021/ACS.JPCA.5B05948.

(2) Zeiger, H. J.; Vidal, J.; Cheng, T. K.; Ippen, E. P.; Dresselhaus, G.; Dresselhaus, M. S. Theory for Displacive Excitation of Coherent Phonons. *Phys. Rev. B* **1992**, *45* (2), 768–778. DOI:10.1103/PhysRevB.45.768.

(3) Sayers, C. J.; Genco, A.; Trovatello, C.; Conte, S. D.; Khaustov, V. O.; Cervantes-Villanueva, J.; Sangalli, D.; Molina-Sanchez, A.; Coletti, C.; Gadermaier, C.; Cerullo, G. Strong Coupling of Coherent Phonons to Excitons in Semiconducting Monolayer MoTe2. *Nano Lett.* **2023**, *23* (20), 9235–9242. DOI:10.1021/ACS.NANOLETT.3C01936.

(4) Kumar, A. T. N.; Rosca, F.; Widom, A.; Champion, P. M. Investigations of Amplitude and Phase Excitation Profiles in Femtosecond Coherence Spectroscopy. *J. Chem. Phys.* **2001**, *114* (2), 701–724. DOI:10.1063/1.1329640.

(5) Xiao, D.; Liu, G. Bin; Feng, W.; Xu, X.; Yao, W. Coupled Spin and Valley Physics in Monolayers of MoS 2 and Other Group-VI Dichalcogenides. *Phys. Rev. Lett.* **2012**, *108* (19). DOI:10.1103/PHYSREVLETT.108.196802.